Advances in Nano Research, *Vol. 9, No. 4 (2020) 221-235*
DOI: https://doi.org/10.12989/anr.2020.9.4.221

Nonlocal dynamic modeling of mass sensors consisting of graphene sheets based on strain gradient theory

Sadok Mehrez[1], Saeed Ali Karati[2], Parnia Taheri DolatAbadi[3], S.N.R. Shah[4], Sikander Azam[5,6], Majid Khorami[7] and Hamid Assilzadeh*[8]

[1]College of Engineering at Al Kharj, Prince Sattam bin Abdulaziz University, 11942, Saudi Arabia
[2]Department of Civil Engineering, Faculty of Engineering, Universiti Malaysia, 50603, Kuala Lumpur, Malaysia
[3]Department of Mechanical, Industrial and Aerospace Engineering, Concordia University, Montreal, QC, H3G 1M8, Canada
[4]Department of Civil Engineering, Mehran University of Engineering and Technology, SZAB Campus, Pakistan
[5]Division of Computational Physics, Institute for Computational Science, Ton Duc Thang University, Ho Chi Minh City, Vietnam
[6]Faculty of Electrical and Electronics Engineering, Ton Duc Thang University, Ho Chi Minh City, Vietnam
[7]Facultad de Arquitectura y Urbanismo, Universidad UTE, Quito, Ecuador
[8]Institute of Research and Development, Duy Tan University, Da Nang 550000, Vietnam

(*Received October 12, 2019, Revised April 24, 2020, Accepted July 1, 2020*)

Abstract. The following composition establishes a nonlocal strain gradient plate model that is essentially related to mass sensors laying on Winkler-Pasternak medium for the vibrational analysis from graphene sheets. To achieve a seemingly accurate study of graphene sheets, the posited theorem actually accommodates two parameters of scale in relation to the gradient of the strain as well as non-local results. Model graphene sheets are known to have double variant shear deformation plate theory without factors from shear correction. By using the principle of Hamilton, to acquire the governing equations of a non-local strain gradient graphene layer on an elastic substrate, Galerkin's method is therefore used to explicate the equations that govern various partition conditions. The influence of diverse factors like the magnetic field as well as the elastic foundation on graphene sheet's vibration characteristics, the number of nanoparticles, nonlocal parameter, nanoparticle mass as well as the length scale parameter had been evaluated.

Keywords: vibration; mass sensor; refined plate theory; graphene sheets; nonlocal strain gradient

1. Introduction

Graphene happens to be an atomic crystal of extraordinary electronic and mechanical properties, which are typically in two dimensions. A lot of nanostructures that depend on carbon like nanobeams, nanoplates and carbon nanotubes are often understood as deformed graphene sheets (Ebrahimi *et al*. 2019). Actually, a nanomaterial and nanostructure research show a thorough examination of graphene sheets which happens to be a fundamental matter. Classic theories from literature works have been used for performing analysis of scale-free plates, yet the scale impact on the nanostructures cannot be studied with small sizes by these theories. Hence, non-local elasticity theory is established in light of the small-scale results. Stark contrast to the local theory where the stress condition during stages provided depends exclusively on the stress state of that level. It is important to note that the stress state at that point depends at all stages on the stress state in the non-local theory. The non-local theory of elasticity has been widely employed in investigating nanoscale structures' mechanical behavior (Ebrahimi and Barati 2016a, b, c, d, e, f). Signs of buckling were observed on single layer graphene sheets exposed to standard in-plane loadings by Pradhan and Murmu (2009). In addition, Pradhan and Kumar (2011) conducted a partially-analytical approach to vibration studies of orthotropic graphene sheets which incorporate non-local effects. The effects of a research conducted by Aksencer and Aydogdu (2011) examine the implementation of the Levy-type method in stability as well as vibrational studies for nanosized plates which include non-local effects. As a result of that, Mohammadi *et al*. (2014) carried out a review of an orthotropic graphene sheet's shear buckling, on elastic substrates which include the thermal loading effect. They demonstrated how graphene sheet vibration reaction is greatly affected by the amount of nanoparticle attached to it. Furthermore, Farajpour *et al*. (2012) investigated the static stability of nonlocal plates which are exposed to standardized edge loads in the plane. On the other hand, Ansari and Sahmani (2013) have implemented simulations of molecular dynamics for investigating the biaxial buckling action for single-layer graphene sheets, dependent on nonlocal elasticity. To derive correct nonlocal parameter values, they compared the findings gathered from molecular dynamics simulations against the nonlocal plate model. According to a higher order shear deformation two-variable theory on the Winkler-Pasternak foundation, Sobhy is studying the vibrational behavior and static bending for single-layered graphene sheets. Furthermore, based on a

*Corresponding author, Ph.D.,
E-mail: hamidassilzadeh@duytan.edu.vn

http://www.techno-press.org/?journal=journal=anr&subpage=5 ISSN: 2287-237X (Print), 2287-2388 (Online)

two-variable non-local refined plate hypothesis, Narendar and Gopalakrishnan (2012) performed a stability study of nanoscale orthotropic plaques which was size-dependent. In their research, they mentioned how the two parameter based polished plate model takes into account the transverse shear effects across the plate depth, thus the implementation of shear correction factors is unnecessary. An investigation was conducted by Murmu *et al*. (2013) which included the effect of unidirectional magnetic fields for single layer nonlocal graphene sheets lying on elastic substrate vibrational behavior. Subsequently, in Bessaim *et al*. (2015) study a nonlocal quasi-3D trigonometric plate model for free micro/nanoscale plate vibration behavior was introduced. Continuously, an examination on free vibrational activity of dual viscoelastic graphene sheets coupled with the visco-pasternak media was completed by Hashemi *et al*. (2015). According to Reddy's theory which explains the higher-order deformation of sheets, Ebrahimi and Shafiei (2016) conducted an investigation where they integrated single-layered graphene sheets inside an elastic medium to understand the impacts of initial shear stress on its vibrational behavior. By implementing the Galerkin strip distributed transfer function technique, Jiang *et al*. (2016) directed an evaluation on vibrational behavior of a mass sensor which was based on a single-layered graphene sheet. Another study worth noting is a study investigated by Arani *et al*. (2016) where they examined non-local vibration of an axially traveling graphene layer sitting beneath longitudinal magnetic field on the orthotropic visco-Pasternak base. Additionally, Sobhy (2016) used the two-variable plate principle to examine the hygro-thermal vibrational action of coupled graphene sheets through an elastic surface. Zenkour (2016) further conducted transient thermal evaluation of graphene sheets derived from non-local elasticity theory on the viscoelastic foundations. Shi *et al*. (2019) investigated the kriging proxy model for graphene uncertainty analysis focused on a finite-element system. Georgantzinos (2017) used computer-aided design/computer-aided computational methods to create the right finite element for an effective mechanical analysis of graphene structures. Georgantzinos *et al*. (2016) used the spring-based finite-element method to evaluate the coupled thermomechanical actions of graphene. Mortazavi *et al*. (2012) performed simulations of molecular dynamics to examine the thickness and chirality impact on the tensile activity of few-layer graphene.

It ought to be referenced that solid is projected in various sorts and shapes including lightweight, high quality, green, permeable and self-combining concrete. Also, Fresh and solidified properties are two sorts of solid qualities while the new properties are alluded to the significant highlights of cement, for example, droop and usefulness. Then again, solidified properties incorporate flexural quality, compressive quality, shear quality, and consumption obstruction. There are different techniques applied to upgrade these properties, for example, cementitious substitution powders the incorporation of the filaments, and surface insurance (Willam 1975, Shariati *et al*. 2010, 2011a, b, d, 2014, 2016, 2019c, f, Hamidian *et al*. 2011, Sinaei *et al*. 2011, Mohammadhassani *et al*. 2014a, c, Arabnejad Khanouki *et al*. 2016, Toghroli *et al*. 2017, 2018b, Heydari *et al*. 2018, Nosrati *et al*. 2018, Shariat *et al*. 2018, Ziaei-Nia *et al*. 2018, Li *et al*. 2019, Luo *et al*. 2019, Safa *et al*. 2019, Sajedi and Shariati 2019, Suhatril *et al*. 2019, Trung *et al*. 2019b, Xie *et al*. 2019, Naghipour *et al*. 2020a, Razavian *et al*. 2020, Zhao *et al*. 2020a, b).

There are various kinds of shaped steel utilized in development applications, for example, hot and cold confined segments. Cold encircled steel associations are utilized in mechanical and capacity applications. Consequently, the presentation of rack associations has been examined in various conditions to improve their exhibition (Shah *et al*. 2015, 2016a, b, c, Chen *et al*. 2019, Naghipour *et al*. 2020b).

The shear quality and burden communicating capability of the composite structures can be improved by shear connectors, which are perhaps the most essential pieces of composite frameworks. Since the shear connectors execution can be influenced by high temperatures, a few examinations have been completed to address the quality loss of these components (Shariati *et al*. 2011c, 2012a, b, e, 2015, Shariati 2013, 2014, Khorramian *et al*. 2016, 2017, Shahabi *et al*. 2016a, b, Tahmasbi *et al*. 2016, Hosseinpour *et al*. 2018, Ismail *et al*. 2018, Nasrollahi *et al*. 2018, Paknahad *et al*. 2018, Wei *et al*. 2018, Davoodnabi *et al*. 2019, Razavian *et al*. 2020, Zhao *et al*. 2019).

Man-made brainpower strategies and exemplary numerical procedures have been consolidated together which made the new half and half calculations so as to tackle the complex issues. In such manner, trial information can be utilized for streamlining and expectation process. It is beneficial to make reference to that few methodologies have been applied in late papers, for example, outrageous learning machine, neural system, and hereditary programming (Shariati *et al*. 2019a, b, d, e, g, 2020a, c, d, e, f, Arabnejad Khanouki *et al*. 2011, Daie *et al*. 2011, Sinaei *et al*. 2012, Mohammadhassani *et al*. 2013, 2014b, 2015, Toghroli 2015, Toghroli *et al*. 2014, 2016, 2018a, Mansouri *et al*. 2016, 2019, Safa *et al*. 2016, 2020, Sadeghi Chahnasir *et al*. 2018, Sari *et al*. 2018, Sedghi *et al*. 2018, Katebi *et al*. 2019, Trung *et al*. 2019a, Xu *et al*. 2019, Armaghani *et al*. 2020, Qi 2020).

Architects ought to think about seismic occasions, which are pulverizing for working in the development procedure. Along these lines, so as to improve the dynamic execution of the structures, various components are planned by analysts. Dampers and diminished segment associations are the two most appropriate components that can be helpful in such manner. What's more, the auxiliary conduct of shear connectors and rack frameworks has been examined through various investigations, for example, monotonic and full cyclic, half-cyclic, and turned around cyclic tests (Arabnejad Khanouki *et al*. 2010, Jalali *et al*. 2012, Shariati 2020, Shariati *et al*. 2012c, d, 2013, 2017, 2018, 2019a, 2020b, g, Khorami *et al*. 2017a, b, Zandi *et al*. 2018, Milovancevic *et al*. 2019).

It really is obvious that almost all former papers regarding graphene sheets have implemented the non-local elasticity principle for the means of catching limited sized results. However, the principle of non-local elasticity has several drawbacks in effective estimation of nanostructural mechanical behavior. Since the principle of non-local elasticity cannot investigate the rise in rigidity found in experimental works and the elasticity of the strain gradients. Lim *et al*. (2015) recently suggested the non-local strain gradient hypothesis to combine all of the longitudinal scales to form one principle. In conjunction with that, the non-local strain gradient hypothesis describes the real effect on the physical as well as mechanical actions of small size systems through the two length scale parameters Li (2016) and Li *et al*. (2016). Ebrahimi and Barati (2017a, b) decided to apply the non-local strain gradient principle of nanobeam analysis. From the information extracted from their study, it can be note that based on the strain gradient and non-local impacts, mechanical properties of nanostructures are relatively influenced by stiffness-hardening and stiffness-softening mechanisms, respectively. Ebrahimi *et al*. (2016) recently expanded the non-local strain gradient principle to analyze nanoplates in order to acquire the wave frequencies over a total of two scale parameters. Thus, it is important that both non-local as well as the strain gradient effects are first incorporated in the graphene sheet's analysis.

Based on a recently established non-local strain gradient principle, a generalized two-variable plate theory is used to analyze vibration activity for single-layer graphene sheets as mass sensors lying on an elastic surface. It is essential to note that the theory integrates two scale variables which correlate to non-local and strain-gradient effects to catch both stiffness-hardening and stiffness-softening influences. The theory of Hamilton is used to achieve a governing equation of a graphene surface with non-local strain gradients. These equations are obtained by the process Galerkin uses to extract the natural frequencies. The vibration activity of graphene sheets has been shown to be greatly affected by non-local parameter, parameter of the length scale, mass of nanoparticles, elastic base and magnetic field in the plane.

2. Governing equations

The principle of the higher-order refined plate theory consists of the area of displacement shown below as

$$u_1(x,y,z) = -z\frac{\partial w_b}{\partial x} - f(z)\frac{\partial w_s}{\partial x} \tag{1}$$

$$u_2(x,y,z) = -z\frac{\partial w_b}{\partial y} - f(z)\frac{\partial w_s}{\partial y} \tag{2}$$

$$u_3(x,y,z) = w_b(x,y) + w_s(x,y) \tag{3}$$

where the current theory has quite a trigonometric function which can be expressed as

$$f(z) = z - \frac{h}{\pi}sin(\frac{\pi z}{h}) \tag{4}$$

Also, w_s as well as w_b both represent the shear and bending transverse displacement, respectively. The present plate model's nonzero strains can be summarized as such

$$\begin{Bmatrix}\varepsilon_x\\ \varepsilon_y\\ \gamma_{xy}\end{Bmatrix} = +z\begin{Bmatrix}\kappa_x^b\\ \kappa_y^b\\ \kappa_{xy}^b\end{Bmatrix} + f(z)\begin{Bmatrix}\kappa_x^s\\ \kappa_y^s\\ \kappa_{xy}^s\end{Bmatrix}$$
$$\begin{Bmatrix}\gamma_{yz}\\ \gamma_{xz}\end{Bmatrix} = g(z)\begin{Bmatrix}\gamma_{yz}^s\\ \gamma_{xz}^s\end{Bmatrix} \tag{5}$$

whereby $g(z) = 1 - df/dz$ and

$$\begin{Bmatrix}\kappa_x^b\\ \kappa_y^b\\ \kappa_{xy}^b\end{Bmatrix} = \begin{Bmatrix}-\dfrac{\partial^2 w_b}{\partial x^2}\\ -\dfrac{\partial^2 w_b}{\partial y^2}\\ -2\dfrac{\partial^2 w_b}{\partial x\partial y}\end{Bmatrix}$$
$$\begin{Bmatrix}\kappa_x^s\\ \kappa_y^s\\ \kappa_{xy}^s\end{Bmatrix} = \begin{Bmatrix}-\dfrac{\partial^2 w_s}{\partial x^2}\\ -\dfrac{\partial^2 w_s}{\partial y^2}\\ -2\dfrac{\partial^2 w_s}{\partial x\partial y}\end{Bmatrix}, \quad \begin{Bmatrix}\gamma_{yz}^s\\ \gamma_{xz}^s\end{Bmatrix} = \begin{Bmatrix}\dfrac{\partial w_s}{\partial y}\\ \dfrac{\partial w_s}{\partial x}\end{Bmatrix} \tag{6}$$

Additionally, this is portrayed by Hamilton's principle

$$\int_0^t \delta(U - T + V)dt = 0 \tag{7}$$

where U is the strain energy, T is kinetic energy and V is work done by external loads. The strain energy variation is quantified by

$$\begin{aligned}\delta U &= \int_v \sigma_{ij}\delta\varepsilon_{ij}dV\\ &= \int_v (\sigma_x\delta\varepsilon_x + \sigma_y\delta\varepsilon_y + \sigma_{xy}\delta\gamma_{xy} + \sigma_{yz}\delta\gamma_{yz} + \sigma_{xz}\delta\gamma_{xz})dV\end{aligned} \tag{8}$$

Substituting Eqs. (5) and (6) into Eq. (8) forms

$$\begin{aligned}\delta U = \int_0^b\int_0^a [- M_x^b\frac{\partial^2\delta w_b}{\partial x^2} - M_x^s\frac{\partial^2\delta w_s}{\partial x^2} - M_y^b\frac{\partial^2\delta w_b}{\partial y^2} -\\ M_y^s\frac{\partial^2\delta w_s}{\partial y^2} - 2M_{xy}^s\frac{\partial^2\delta w_s}{\partial x\partial y} + Q_{yz}\frac{\partial\delta w_s}{\partial y} + Q_{xz}\frac{\partial\delta w_s}{\partial x}]dxdy\end{aligned} \tag{9}$$

wherein

$$\begin{aligned}(M_i^b, M_i^s) &= \int_{-h/2}^{h/2}(z,f)\sigma_i\,dz, i = (x,y,xy)\\ Q_i &= \int_{-h/2}^{h/2} g\sigma_i\,dz, i = (xz,yz)\end{aligned} \tag{10}$$

The variation of the work done from applied loads can be expressed through

$$\begin{aligned}\delta V = \int_0^b\int_0^a (N_x^0\frac{\partial(w_b + w_s)}{\partial x}\frac{\partial\delta(w_b + w_s)}{\partial x}\\ + N_y^0\frac{\partial(w_b + w_s)}{\partial y}\frac{\partial\delta(w_b + w_s)}{\partial y} + 2\delta N_{xy}^0\end{aligned} \tag{11a}$$

$$\frac{\partial(w_b+w_s)}{\partial x}\frac{\partial(w_b+w_s)}{\partial y}-k_w\delta(w_b+w_s)$$
$$+q_{particle}\delta(w_b+w_s)+\left(\eta h H_x^2+k_p\right)$$
$$(\frac{\partial(w_b+w_s)}{\partial x}\frac{\partial\delta(w_b+w_s)}{\partial x}+\frac{\partial(w_b+w_s)}{\partial y}\qquad(11a)$$
$$\frac{\partial\delta(w_b+w_s)}{\partial y}))dxdy$$

where N_x^0, N_y^0, N_{xy}^0 are in-plane applied loads; k_w and k_p are Winkler and Pasternak constants. Additionally, η is magnetic parliamentary. Also, $q_{particle}$ happens to be the transverse force because of attached nanoparticles (more like a bacterium, molecular or buckyball) which has a mass m_c that happens to be adhered to the location $x = x_0$, $y = y_0$.

$$q_{particle}=-\sum_{j=1}^{N}m_j\,\delta(x-x_j,y-y_j)\frac{\partial^2 w}{\partial t^2}\qquad(11b)$$

in which m_j is the mass of jth attached particle, while N is the amount of concentrated masses. Furthermore, $\delta(x-x_j)$ is Dirac delta function outlined by

$$\delta(x-x_j)=\begin{cases}\infty & x\neq x_j\\ 0 & x=x_j\end{cases}\qquad(11c)$$

The kinetic energy's variation is calculated as

$$\delta K=\int_0^b\int_0^a[\,I_0(\frac{\partial(w_b+w_s)}{\partial t}\frac{\partial\delta(w_b+w_s)}{\partial t})$$
$$+I_2\left(\frac{\partial w_b}{\partial x\partial t}\frac{\partial\delta w_b}{\partial x\partial t}+\frac{\partial w_b}{\partial y\partial t}\frac{\partial\delta w_b}{\partial y\partial t}\right)+K_2\left(\frac{\partial w_s}{\partial x\partial t}\right.$$
$$\left.\frac{\partial\delta w_s}{\partial x\partial t}+\frac{\partial w_s}{\partial y\partial t}\frac{\partial\delta w_s}{\partial y\partial t}\right)+J_2(\frac{\partial w_b}{\partial x\partial t}\frac{\partial\delta w_s}{\partial x\partial t}+\frac{\partial w_s}{\partial x\partial t}\qquad(12)$$
$$\frac{\partial\delta w_b}{\partial x\partial t}+\frac{\partial w_b}{\partial y\partial t}\frac{\partial\delta w_s}{\partial y\partial t}+\frac{\partial w_s}{\partial y\partial t}\frac{\partial\delta w_b}{\partial y\partial t})]dxdy$$

wherein

$$(I_0,I_2,J_2,K_2)=\int_{-h/2}^{h/2}(1,z^2,zf,f^2)\rho\,dz\qquad(13)$$

Through inputting Eqs. (19)-(22) into Eq. (17) as well as setting the coefficients of δu, δv, δw_b and δw_s to zero, the following Euler-Lagrange expressions should be attained.

$$\frac{\partial^2 M_x^b}{\partial x^2}+2\frac{\partial^2 M_{xy}^b}{\partial x\partial y}+\frac{\partial^2 M_y^b}{\partial y^2}-(N^T+N^H-\eta h H_x^2)\nabla^2$$
$$(w_b+w_s)+k_p\left[\frac{\partial^2(w_b+w_s)}{\partial x^2}+\frac{\partial^2(w_b+w_s)}{\partial y^2}\right]$$
$$-k_w(w_b+w_s)-\sum_{j=1}^{N}m_j\,\delta\left(x-x_j,y-y_j\right)\frac{\partial^2 w}{\partial t^2}\qquad(14)$$
$$=I_0\frac{\partial^2(w_b+w_s)}{\partial t^2}-I_2\nabla^2(\frac{\partial^2 w_b}{\partial t^2})-J_2\nabla^2(\frac{\partial^2 w_s}{\partial t^2})$$

$$\frac{\partial^2 M_x^s}{\partial x^2}+2\frac{\partial^2 M_{xy}^s}{\partial x\partial y}+\frac{\partial^2 M_y^s}{\partial y^2}+\frac{\partial Q_{xz}}{\partial x}+\frac{\partial Q_{yz}}{\partial y}-(N^T\qquad(15)$$
$$+N^H-\eta h H_x^2)\nabla^2(w_b+w_s)\;+k_p[\frac{\partial^2(w_b+w_s)}{\partial x^2}$$
$$+\frac{\partial^2(w_b+w_s)}{\partial y^2}]-k_w(w_b+w_s)\;-\sum_{j=1}^{N}m_j\,\delta(x-x_j,$$
$$y-y_j)\frac{\partial^2 w}{\partial t^2}=I_0\frac{\partial^2(w_b+w_s)}{\partial t^2}-J_2\nabla^2(\frac{\partial^2 w_b}{\partial t^2})\qquad(15)$$
$$-K_2\nabla^2(\frac{\partial^2 w_s}{\partial t^2})$$

2.1 Nonlocal strain gradient nanoplate model

The recently created nonlocal strain gradient theory considers the nonlocal stress field as well as the strain gradient effects through presenting two scale parameters. This theory describes the stress field as

$$\sigma_{ij}=\sigma_{ij}^{(0)}-\frac{d\sigma_{ij}^{(1)}}{dx}\qquad(18)$$

in which the stresses $\sigma_{xx}^{(0)}$and $\sigma_{xx}^{(1)}$correspond to strain ε_{xx} along with strain gradient $\varepsilon_{xx,x}$, respectively through

$$\sigma_{ij}^{(0)}=\int_0^L C_{ijkl}\,\alpha_0(x,x',e_0a)\varepsilon_{kl}'(x')dx'\qquad(19)$$

$$\sigma_{ij}^{(1)}=l^2\int_0^L C_{ijkl}\,\alpha_1(x,x',e_1a)\varepsilon_{kl,x}'(x')dx'\qquad(20)$$

whereby C_{ijkl} is the elastic coefficients and e_0a alongside e_1a apprehends the nonlocal effects and l take into consideration the effects of the strain gradient. The constitutive relation of nonlocal strain gradient theory contains the mentioned form below, when the nonlocal functions $\alpha_0(x,x',e_0a)$ and $\alpha_1(x,x',e_1a)$ satisfy the conditions created by Eringen (1983)

$$[1-(e_1a)^2\nabla^2][1-(e_0a)^2\nabla^2]\sigma_{ij}$$
$$=C_{ijkl}[1-(e_1a)^2\nabla^2]\varepsilon_{kl}-C_{ijkl}l^2[1(e_0a)^2\nabla^2]\nabla^2\varepsilon_{kl}\qquad(21)$$

where ∇^2 signifies the Laplacian operator. When taking into account that $e_1=e_0=e$, the general constitutive relation in Eq. (21) ends up as

$$[1-(ea)^2\nabla^2]\sigma_{ij}=C_{ijkl}[1-l^2\nabla^2]\varepsilon_{kl}\qquad(22)$$

Lastly, the constitutive relations of nonlocal strain gradient theory may get portrayed through

$$(1-\mu\nabla^2)\begin{Bmatrix}\sigma_x\\ \sigma_y\\ \sigma_{xy}\\ \sigma_{yz}\\ \sigma_{xz}\end{Bmatrix}=(1-\lambda\nabla^2)\begin{pmatrix}Q_{11}&Q_{12}&0&0&0\\ Q_{12}&Q_{22}&0&0&0\\ 0&0&Q_{66}&0&0\\ 0&0&0&Q_{44}&0\\ 0&0&0&0&Q_{55}\end{pmatrix}\begin{Bmatrix}\varepsilon_x\\ \varepsilon_y\\ \gamma_{xy}\\ \gamma_{yz}\\ \gamma_{xz}\end{Bmatrix}\qquad(23)$$

where

$$Q_{11}=Q_{22}=\frac{E}{1-\upsilon^2},\qquad Q_{12}=\upsilon Q_{11}$$
$$Q_{44}=Q_{55}=Q_{66}=\frac{E}{2(1+\upsilon)} \tag{24}$$

Inputting Eq. (10) in Eq. (23) gives

$$(1-(ea)^2\nabla^2)\begin{Bmatrix}M_x^b\\M_y^b\\M_{xy}^b\end{Bmatrix}=(1-l^2\nabla^2)\left[\begin{pmatrix}D_{11}&D_{12}&0\\D_{12}&D_{22}&0\\0&0&D_{66}\end{pmatrix}\begin{Bmatrix}-\frac{\partial^2 w_b}{\partial x^2}\\-\frac{\partial^2 w_b}{\partial y^2}\\-2\frac{\partial^2 w_b}{\partial x\partial y}\end{Bmatrix}+\begin{pmatrix}D_{11}^s&D_{12}^s&0\\D_{12}^s&D_{22}^s&0\\0&0&D_{66}^s\end{pmatrix}\begin{Bmatrix}-\frac{\partial^2 w_s}{\partial x^2}\\-\frac{\partial^2 w_s}{\partial y^2}\\-2\frac{\partial^2 w_s}{\partial x\partial y}\end{Bmatrix}\right] \tag{25}$$

$$(1-(ea)^2\nabla^2)\begin{Bmatrix}M_x^s\\M_y^s\\M_{xy}^s\end{Bmatrix}=(1-l^2\nabla^2)\left[\begin{pmatrix}D_{11}^s&D_{12}^s&0\\D_{12}^s&D_{22}^s&0\\0&0&D_{66}^s\end{pmatrix}\begin{Bmatrix}-\frac{\partial^2 w_b}{\partial x^2}\\-\frac{\partial^2 w_b}{\partial y^2}\\-2\frac{\partial^2 w_b}{\partial x\partial y}\end{Bmatrix}+\begin{pmatrix}H_{11}^s&H_{12}^s&0\\H_{12}^s&H_{22}^s&0\\0&0&H_{66}^s\end{pmatrix}\begin{Bmatrix}-\frac{\partial^2 w_s}{\partial x^2}\\-\frac{\partial^2 w_s}{\partial y^2}\\-2\frac{\partial^2 w_s}{\partial x\partial y}\end{Bmatrix}\right] \tag{26}$$

$$(1-(ea)^2\nabla^2)\begin{Bmatrix}Q_x\\Q_y\end{Bmatrix}=(1-l^2\nabla^2)[\begin{pmatrix}A_{44}^s&0\\0&A_{55}^s\end{pmatrix}\begin{Bmatrix}\frac{\partial w_s}{\partial x}\\\frac{\partial w_s}{\partial y}\end{Bmatrix}] \tag{27}$$

$$\begin{Bmatrix}D_{11},D_{11}^s,H_{11}^s\\D_{12},D_{12}^s,H_{12}^s\\D_{66},D_{66}^s,H_{66}^s\end{Bmatrix}=\int_{-h/2}^{h/2}Q_{11}(z^2,zf,f^2)\begin{Bmatrix}1\\\nu\\\frac{1-\nu}{2}\end{Bmatrix}dz \tag{28}$$

$$A_{44}^s=A_{55}^s=\int_{-h/2}^{h/2}g^2\frac{E}{2(1+\upsilon)}dz \tag{29}$$

The governing equations of nonlocal strain gradient graphene sheet based on the displacement are gathered by placing Eqs. (25)-(27), into Eqs. (14)-(15) as shown below.

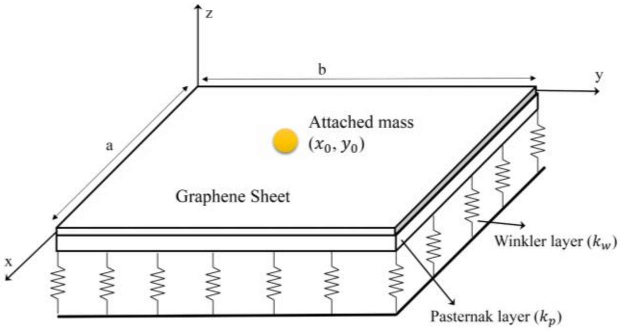

Fig. 1 Configuration of graphene sheet laying on elastic substrate

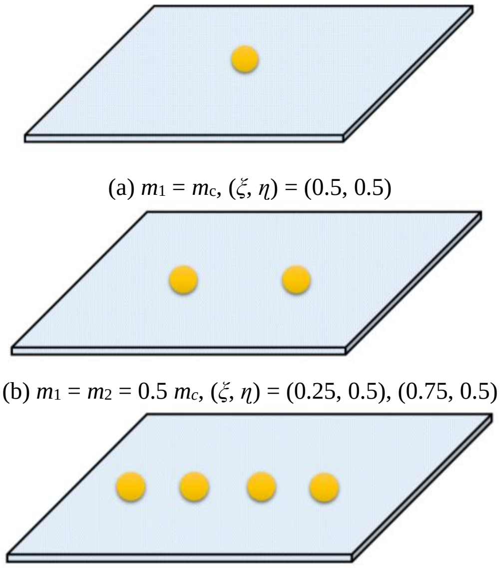

(a) $m_1 = m_c$, $(\xi, \eta) = (0.5, 0.5)$

(b) $m_1 = m_2 = 0.5\, m_c$, $(\xi, \eta) = (0.25, 0.5), (0.75, 0.5)$

(c) $m_1 = m_2 = m_3 = m_4 = 0.25\, m_c$, $(\xi, \eta) = (0.2, 0.5), (0.4, 0.5), (0.6, 0.5), (0.8, 0.5)$

Fig. 2 Detailed distributions of nanoparticles and their relative mass

3. Solution by Galerkin's approach

For this portion, Galerkin's approach of solving the governing equations for non-local strain gradient graphene sheets is enforced. Therefore, the field of displacement may get computed as

$$\begin{aligned}&-D_{11}[\frac{\partial^4 w_b}{\partial x^4}-l^2(\frac{\partial^6 w_b}{\partial x^6}+\frac{\partial^6 w_b}{\partial x^4\partial y^2})]-2(D_{12}+2D_{66})[\frac{\partial^4 w_b}{\partial x^2\partial y^2}-l^2(\frac{\partial^6 w_b}{\partial x^4\partial y^2}+\frac{\partial^6 w_b}{\partial x^2\partial y^4})]-D_{22}[\frac{\partial^4 w_b}{\partial y^4}-l^2(\frac{\partial^6 w_b}{\partial y^6}\\&+\frac{\partial^6 w_b}{\partial y^4\partial x^2})]-D_{11}^s[\frac{\partial^4 w_s}{\partial x^4}-l^2(\frac{\partial^6 w_s}{\partial x^6}+\frac{\partial^6 w_s}{\partial x^4\partial y^2})]-2(D_{12}^s+2D_{66}^s)[\frac{\partial^4 w_s}{\partial x^2\partial y^2}-l^2(\frac{\partial^6 w_s}{\partial x^4\partial y^2}+\frac{\partial^6 w_s}{\partial x^2\partial y^4})]-D_{22}^s[\frac{\partial^4 w_s}{\partial y^4}\\&-l^2(\frac{\partial^6 w_s}{\partial y^6}+\frac{\partial^6 w_s}{\partial y^4\partial x^2})]-I_0[\frac{\partial^2(w_b+w_s)}{\partial t^2}-(ea)^2(\frac{\partial^4(w_b+w_s)}{\partial t^2\partial x^2}+\frac{\partial^4(w_b+w_s)}{\partial t^2\partial y^2})]+I_2[\frac{\partial^4 w_b}{\partial x^2\partial t^2}+\frac{\partial^4 w_b}{\partial y^2\partial t^2}-\mu\\&(\frac{\partial^6 w_b}{\partial t^2\partial x^4}+2\frac{\partial^6 w_b}{\partial t^2\partial x^2\partial y^2}+\frac{\partial^6 w_b}{\partial t^2\partial y^4})]+J_2[\frac{\partial^4 w_s}{\partial x^2\partial t^2}+\frac{\partial^4 w_s}{\partial y^2\partial t^2}-(ea)^2(\frac{\partial^6 w_s}{\partial t^2\partial x^4}+2\frac{\partial^6 w_s}{\partial t^2\partial x^2\partial y^2}+\frac{\partial^6 w_s}{\partial t^2\partial y^4})]\\&+(\eta h H_x^2)[\frac{\partial^2(w_b+w_s)}{\partial x^2}+\frac{\partial^2(w_b+w_s)}{\partial y^2}-(ea)^2(\frac{\partial^4(w_b+w_s)}{\partial x^4}+2\frac{\partial^4(w_b+w_s)}{\partial x^2\partial y^2}+\frac{\partial^4(w_b+w_s)}{\partial y^4})]+(1-(ea)^2\frac{\partial^2}{\partial x^2}\\&+\frac{\partial^2}{\partial y^2})[k_p[\frac{\partial^2(w_b+w_s)}{\partial x^2}+\frac{\partial^2(w_b+w_s)}{\partial y^2}]-k_w(w_b+w_s)-\sum_{j=1}^{N}m_j\,\delta(x-x_j,y-y_j)\frac{\partial^2 w}{\partial t^2}]=0\end{aligned} \tag{30}$$

$$
\begin{aligned}
& D_{11}^{s}[\frac{\partial^4 w_b}{\partial x^4} - l^2(\frac{\partial^6 w_b}{\partial x^6} + \frac{\partial^6 w_b}{\partial x^4 \partial y^2})] + A_{55}^{s}[\frac{\partial^2 w_s}{\partial x^2} - l^2(\frac{\partial^4 w_s}{\partial x^4} + \frac{\partial^4 w_s}{\partial x^2 \partial y^2})] + A_{44}^{s}[\frac{\partial^2 w_s}{\partial y^2} - l^2(\frac{\partial^4 w_s}{\partial y^4} + \frac{\partial^4 w_s}{\partial y^2 \partial x^2})] - 2(D_{12}^{s} \\
& + 2D_{66}^{s})[\frac{\partial^4 w_b}{\partial x^2 \partial y^2} - l^2(\frac{\partial^6 w_b}{\partial x^4 \partial y^2} + \frac{\partial^6 w_b}{\partial x^2 \partial y^4})] - D_{22}^{s}[\frac{\partial^4 w_b}{\partial y^4} - l^2(\frac{\partial^6 w_b}{\partial y^6} + \frac{\partial^6 w_b}{\partial y^4 \partial x^2})] - H_{11}^{s}[\frac{\partial^4 w_s}{\partial x^4} - l^2(\frac{\partial^6 w_s}{\partial x^6} + \frac{\partial^6 w_s}{\partial x^4 \partial y^2})] \\
& - 2(H_{12}^{s} + 2H_{66}^{s})[\frac{\partial^4 w_s}{\partial x^2 \partial y^2} - l^2(\frac{\partial^6 w_s}{\partial x^4 \partial y^2} + \frac{\partial^6 w_s}{\partial x^2 \partial y^4})] - H_{22}^{s}[\frac{\partial^4 w_s}{\partial y^4} - l^2(\frac{\partial^6 w_s}{\partial y^6} + \frac{\partial^6 w_s}{\partial y^4 \partial x^2})] - I_0[\frac{\partial^2 (w_b + w_s)}{\partial t^2} \\
& -(ea)^2(\frac{\partial^4 (w_b + w_s)}{\partial t^2 \partial x^2} + \frac{\partial^4 (w_b + w_s)}{\partial t^2 \partial y^2})] + J_2[\frac{\partial^4 w_b}{\partial x^2 \partial t^2} + \frac{\partial^4 w_b}{\partial y^2 \partial t^2} - (ea)^2(\frac{\partial^6 w_b}{\partial t^2 \partial x^4} + 2\frac{\partial^6 w_b}{\partial t^2 \partial x^2 \partial y^2} + \frac{\partial^6 w_b}{\partial t^2 \partial y^4})] + K_2 \\
& [\frac{\partial^4 w_s}{\partial x^2 \partial t^2} + \frac{\partial^4 w_s}{\partial y^2 \partial t^2} - (ea)^2(\frac{\partial^6 w_s}{\partial t^2 \partial x^4} + 2\frac{\partial^6 w_s}{\partial t^2 \partial x^2 \partial y^2} + \frac{\partial^6 w_s}{\partial t^2 \partial y^4})] + \eta h H_x^2[\frac{\partial^2 (w_b + w_s)}{\partial x^2} + \frac{\partial^2 (w_b + w_s)}{\partial y^2} - (ea)^2 \\
& (\frac{\partial^4 (w_b + w_s)}{\partial x^4} + 2\frac{\partial^4 (w_b + w_s)}{\partial x^2 \partial y^2} + (1 - (ea)^2(\frac{\partial^2}{\partial x^2} + \frac{\partial^2}{\partial y^2}))[k_p[\frac{\partial^2 (w_b + w_s)}{\partial x^2} + \frac{\partial^2 (w_b + w_s)}{\partial y^2}] - k_w(w_b + w_s) \\
& - \sum_{j=1}^{N} m_j\, \delta(x - x_j, y - y_j) \frac{\partial^2 w}{\partial t^2}] = 0
\end{aligned} \tag{31}
$$

$$w_b = \sum_{m=1}^{\infty} \sum_{n=1}^{\infty} W_{bmn} \Phi_{bm}(x)\, \Psi_{bn}(y) e^{i\omega_n t} \tag{32}$$

$$w_s = \sum_{m=1}^{\infty} \sum_{n=1}^{\infty} W_{smn} \Phi_{sm}(x)\, \Psi_{sn}(y) e^{i\omega_n t} \tag{33}$$

whereby W_{bmn}, W_{smn} are the unknown coefficients while the functions Φ_m as well as Ψ_n satisfy boundary conditions. According to present plate model, the boundary conditions are

$$
\begin{aligned}
& w_b = w_s = 0 \\
& \frac{\partial^2 w_b}{\partial x^2} = \frac{\partial^2 w_s}{\partial x^2} = \frac{\partial^2 w_b}{\partial y^2} = \frac{\partial^2 w_s}{\partial y^2} = 0 \quad \text{simply-supported edge}
\end{aligned} \tag{34}
$$

Inserting Eqs. (32) and (33) into Eqs. (30)-(31) while ensuring to multiple both sides of the equations through $\Phi_{im}\Psi_{in}$ $(i = b, s)$ and incorporating over the entire region results in the simultaneous equations shown below.

$$
\begin{aligned}
& \int_0^b \int_0^a \Phi_{bm}\Psi_{bn}[-D_{11}[\frac{\partial^4 \Phi_{bm}}{\partial x^4}\Psi_{bn} - l^2(\frac{\partial^6 \Phi_{bm}}{\partial x^6}\Psi_{bn} + \frac{\partial^4 \Phi_{bm}}{\partial x^4} \\
& \frac{\partial^2 \Psi_{bn}}{\partial y^2})] - 2(D_{12} + 2D_{66})[\frac{\partial^2 \Phi_{bm}}{\partial x^2}\frac{\partial^2 \Psi_{bn}}{\partial y^2} - l^2(\frac{\partial^4 \Phi_{bm}}{\partial x^4}\frac{\partial^2 \Psi_{bn}}{\partial y^2} \\
& + \frac{\partial^2 \Phi_{bm}}{\partial x^2}\frac{\partial^4 \Psi_{bn}}{\partial y^4})] - D_{22}[\frac{\partial^4 \Psi_{bm}}{\partial y^4}\Phi_{bn} - l^2(\frac{\partial^6 \Psi_{bm}}{\partial y^6}\Phi_{bn} + \frac{\partial^2 \Phi_{bm}}{\partial x^2} \\
& \frac{\partial^4 \Psi_{bn}}{\partial y^4})] - D_{11}^{s}[\frac{\partial^4 \Phi_{sm}}{\partial x^4}\Psi_{sn} - l^2(\frac{\partial^6 \Phi_{sm}}{\partial x^6}\Psi_{sn} + \frac{\partial^4 \Phi_{sm}}{\partial x^4}\frac{\partial^2 \Psi_{sn}}{\partial y^2})] \\
& - 2(D_{12}^{s} + 2D_{66}^{s})[\frac{\partial^2 \Phi_{sm}}{\partial x^2}\frac{\partial^2 \Psi_{sn}}{\partial y^2} - l^2(\frac{\partial^4 \Phi_{sm}}{\partial x^4}\frac{\partial^2 \Psi_{sn}}{\partial y^2} + \frac{\partial^2 \Phi_{sm}}{\partial x^2} \\
& \frac{\partial^4 \Psi_{sn}}{\partial y^4})] - D_{22}^{s}[\frac{\partial^4 \Psi_{sm}}{\partial y^4}\Phi_{sn} - \lambda(\frac{\partial^6 \Psi_{sm}}{\partial y^6}\Phi_{sn} + \frac{\partial^2 \Phi_{sm}}{\partial x^2}\frac{\partial^4 \Psi_{sn}}{\partial y^4})] \\
& + I_0\omega^2[(\Phi_{bm}\Psi_{bn} + \Phi_{sm}\Psi_{sn}) - (ea)^2(\frac{\partial^2 \Phi_{bm}}{\partial x^2}\Psi_{bn} + \frac{\partial^2 \Phi_{sm}}{\partial x^2}\Psi_{sn} \\
& + \frac{\partial^2 \Psi_{sm}}{\partial y^2}\Phi_{sn} + \frac{\partial^2 \Psi_{bm}}{\partial y^2}\Phi_{bn})] - I_2\omega^2[\frac{\partial^2 \Phi_{bm}}{\partial x^2}\Psi_{bn} + \frac{\partial^2 \Psi_{bm}}{\partial y^2}\Phi_{bn} \\
& - (ea)^2(\frac{\partial^4 \Phi_{bm}}{\partial x^4}\Psi_{bn} + 2\frac{\partial^2 \Phi_{bm}}{\partial x^2}\frac{\partial^2 \Psi_{bn}}{\partial y^2} + \frac{\partial^b \Psi_{sm}}{\partial y^4}\Phi_{bn})] - J_2\omega^2 \\
& [\frac{\partial^2 \Phi_{sm}}{\partial x^2}\Psi_{sn} + \frac{\partial^2 \Psi_{sm}}{\partial y^2}\Phi_{sn} - (ea)^2(\frac{\partial^4 \Phi_{sm}}{\partial x^4}\Psi_{sn} + 2\frac{\partial^2 \Phi_{sm}}{\partial x^2}\frac{\partial^2 \Psi_{sn}}{\partial y^2} \\
& + \frac{\partial^4 \Psi_{sm}}{\partial y^4}\Phi_{sn})] + \eta\, h H_x^2[\frac{\partial^2 \Phi_{bm}}{\partial x^2}\Psi_{bn} + \frac{\partial^2 \Phi_{sm}}{\partial x^2}\Psi_{sn} + \frac{\partial^2 \Psi_{sm}}{\partial y^2}\Phi_{sn} \\
& + \frac{\partial^2 \Psi_{bm}}{\partial y^2}\Phi_{bn} - (ea)^2(\frac{\partial^4 \Phi_{bm}}{\partial x^4}\Psi_{bn} + \frac{\partial^4 \Phi_{sm}}{\partial x^4}\Psi_{sn} + 2(\frac{\partial^2 \Phi_{bm}}{\partial x^2}
\end{aligned} \tag{35}
$$

$$
\begin{aligned}
& \frac{\partial^2 \Psi_{bn}}{\partial y^2} + \frac{\partial^2 \Phi_{sm}}{\partial x^2}\frac{\partial^2 \Psi_{sn}}{\partial y^2}) + \frac{\partial^4 \Psi_{sm}}{\partial y^4}\Phi_{sn} + \frac{\partial^4 \Psi_{bm}}{\partial y^4}\Phi_{bn}) + k_p(1 \\
& - (ea)^2(\frac{\partial}{\partial x^2} + \frac{\partial}{\partial x^2}))[\frac{\partial^2 \Phi_{bm}}{\partial x^2}\Psi_{bn} + \frac{\partial^2 \Phi_{sm}}{\partial x^2}\Psi_{sn} + \frac{\partial^2 \Psi_{sm}}{\partial y^2}\Phi_{sn} \\
& + \frac{\partial^2 \Psi_{bm}}{\partial y^2}\Phi_{bn}] - k_w(1 - (ea)^2(\frac{\partial}{\partial x^2} + \frac{\partial}{\partial x^2}))(\Phi_{bm}\Psi_{bn} \\
& + \Phi_{sm}\Psi_{sn}) + \omega^2 \frac{4m_c}{ab} sin^2(\pi\frac{x_0}{a})\, sin^2(\pi\frac{y_0}{b})(1 - \mu(\frac{\partial}{\partial x^2} \\
& + \frac{\partial}{\partial x^2}))(\Phi_{bm}\Psi_{bn} + \Phi_{sm}\Psi_{sn})]dxdy = 0
\end{aligned} \tag{35}
$$

$$
\begin{aligned}
& \int_0^b \int_0^a \Phi_{sm}\Psi_{sn}[-D_{11}^{s}[\frac{\partial^4 \Phi_{bm}}{\partial x^4}\Psi_{bn} - l^2(\frac{\partial^6 \Phi_{bm}}{\partial x^6}\Psi_{bn} + \frac{\partial^4 \Phi_{bm}}{\partial x^4} \\
& \frac{\partial^2 \Psi_{bn}}{\partial y^2})] - 2(D_{12}^{s} + 2D_{66}^{s})[\frac{\partial^2 \Phi_{bm}}{\partial x^2}\frac{\partial^2 \Psi_{bn}}{\partial y^2} - l^2(\frac{\partial^4 \Phi_{bm}}{\partial x^4}\frac{\partial^2 \Psi_{bn}}{\partial y^2} \\
& + \frac{\partial^2 \Phi_{bm}}{\partial x^2}\frac{\partial^4 \Psi_{bn}}{\partial y^4})] - D_{22}^{s}[\frac{\partial^4 \Psi_{bm}}{\partial y^4}\Phi_{bn} - l^2(\frac{\partial^6 \Psi_{bm}}{\partial y^6}\Phi_{bn} + \frac{\partial^2 \Phi_{bm}}{\partial x^2} \\
& \frac{\partial^4 \Psi_{bn}}{\partial y^4})] - H_{11}^{s}\left[\frac{\partial^4 \Phi_{sm}}{\partial x^4}\Psi_{sn} - l^2\left(\frac{\partial^6 \Phi_{sm}}{\partial x^6}\Psi_{sn} + \frac{\partial^4 \Phi_{sm}}{\partial x^4}\frac{\partial^2 \Psi_{sn}}{\partial y^2}\right)\right] \\
& -2(H_{12}^{s} + 2H_{66}^{s})[\frac{\partial^2 \Phi_{sm}}{\partial x^2}\frac{\partial^2 \Psi_{sn}}{\partial y^2} - l^2(\frac{\partial^4 \Phi_{sm}}{\partial x^4}\frac{\partial^2 \Psi_{sn}}{\partial y^2} + \frac{\partial^2 \Phi_{sm}}{\partial x^2} \\
& \frac{\partial^4 \Psi_{sn}}{\partial y^4})] - H_{22}^{s}\left[\frac{\partial^4 \Psi_{sm}}{\partial y^4}\Phi_{sn} - l^2\left(\frac{\partial^6 \Psi_{sm}}{\partial y^6}\Phi_{sn} + \frac{\partial^2 \Phi_{sm}}{\partial x^2}\frac{\partial^4 \Psi_{sn}}{\partial y^4}\right)\right] \\
& + I_0\omega^2[\Phi_{bm}\Psi_{bn} - (ea)^2(\frac{\partial^2 \Phi_{bm}}{\partial x^2}\Psi_{bn} + \frac{\partial^2 \Phi_{sm}}{\partial x^2}\Psi_{sn} + \frac{\partial^2 \Psi_{sm}}{\partial y^2}\Phi_{sn} \\
& + \frac{\partial^2 \Psi_{bm}}{\partial y^2}\Phi_{bn})] - J_2\omega^2[\frac{\partial^2 \Phi_{bm}}{\partial x^2}\Psi_{bn} + \frac{\partial^2 \Psi_{bm}}{\partial y^2}\Phi_{bn} - (ea)^2 \\
& (\frac{\partial^4 \Phi_{bm}}{\partial x^4}\Psi_{bn} + 2\frac{\partial^2 \Phi_{bm}}{\partial x^2}\frac{\partial^2 \Psi_{bn}}{\partial y^2} + \frac{\partial^b \Psi_{sm}}{\partial y^4}\Phi_{bn})] - K_2\omega^2 \\
& [\frac{\partial^2 \Phi_{sm}}{\partial x^2}\Psi_{sn} + \frac{\partial^2 \Psi_{sm}}{\partial y^2}\Phi_{sn} - (ea)^2(\frac{\partial^4 \Phi_{sm}}{\partial x^4}\Psi_{sn} + 2\frac{\partial^2 \Phi_{sm}}{\partial x^2}\frac{\partial^2 \Psi_{sn}}{\partial y^2} \\
& + \frac{\partial^4 \Psi_{sm}}{\partial y^4}\Phi_{sn})] + \eta h H_x^2[\frac{\partial^2 \Phi_{bm}}{\partial x^2}\Psi_{bn} + \frac{\partial^2 \Phi_{sm}}{\partial x^2}\Psi_{sn} + \frac{\partial^2 \Psi_{sm}}{\partial y^2}\Phi_{sn} \\
& + \frac{\partial^2 \Psi_{bm}}{\partial y^2}\Phi_{bn} - (ea)^2(\frac{\partial^4 \Phi_{bm}}{\partial x^4}\Psi_{bn} + \frac{\partial^4 \Phi_{sm}}{\partial x^4}\Psi_{sn} + 2(\frac{\partial^2 \Phi_{bm}}{\partial x^2} \\
& \frac{\partial^2 \Psi_{bn}}{\partial y^2} + \frac{\partial^2 \Phi_{sm}}{\partial x^2}\frac{\partial^2 \Psi_{sn}}{\partial y^2}) + \frac{\partial^4 \Psi_{sm}}{\partial y^4}\Phi_{sn} + \frac{\partial^4 \Psi_{bm}}{\partial y^4}\Phi_{bn}) + A_{55}^{s} \\
& [\frac{\partial^2 \Phi_{sm}}{\partial x^2}\Psi_{sn} - l^2(\frac{\partial^4 \Phi_{sm}}{\partial x^4}\Psi_{sn} + \frac{\partial^2 \Phi_{sm}}{\partial x^2}\frac{\partial^2 \Psi_{sn}}{\partial y^2})] + A_{44}^{s}[\frac{\partial^2 \Psi_{sm}}{\partial y^2}\Phi_{sn} \\
& - l^2(\frac{\partial^4 \Psi_{sm}}{\partial y^4}\Phi_{sn} + \frac{\partial^2 \Phi_{sm}}{\partial x^2}\frac{\partial^2 \Psi_{sn}}{\partial y^2}) + k_p(1 - (ea)^2(\frac{\partial}{\partial x^2} + \frac{\partial}{\partial x^2})) \\
& [\frac{\partial^2 \Phi_{bm}}{\partial x^2}\Psi_{bn} + \frac{\partial^2 \Phi_{sm}}{\partial x^2}\Psi_{sn} + \frac{\partial^2 \Psi_{sm}}{\partial y^2}\Phi_{sn} + \frac{\partial^2 \Psi_{bm}}{\partial y^2}\Phi_{bn}] - k_w(1 \\
& - \left(ea)^2\left(\frac{\partial}{\partial x^2} + \frac{\partial}{\partial x^2}\right)\right)(\Phi_{bm}\Psi_{bn} + \Phi_{sm}\Psi_{sn}) + \omega^2\frac{4m_c}{ab} \\
& sin^2(\pi\frac{x_0}{a})\, sin^2(\pi\frac{y_0}{b})(1 - (ea)^2(\frac{\partial}{\partial x^2} + \frac{\partial}{\partial x^2}))(\Phi_{bm}\Psi_{bn} \\
& + \Phi_{sm}\Psi_{sn})]dxdy = 0
\end{aligned} \tag{36}
$$

Table 1 Comparison of natural frequency of a graphene sheet for various nonlocal and foundation parameters (a/h = 10)

μ	$K_w = 0$, $K_p = 0$		$K_w = 100$, $K_p = 0$		$K_w = 0$, $K_p = 20$	
	Sobhy (2014)	Present	Sobhy (2014)	Present	Sobhy (2014)	Present
0	1.93861	1.93861	2.18396	2.18396	2.7841	2.78410
1	1.17816	1.17816	1.54903	1.54903	2.31969	2.31969
2	0.92261	0.92261	1.36479	1.36479	2.20092	2.20092
3	0.78347	0.78347	1.27485	1.27485	2.14629	2.14629
4	0.69279	0.69279	1.22122	1.22122	2.11486	2.11486

The function Φ_m for simply-supported boundary conditions is outlined by

$$\text{SS:}\ \Phi_m(x) = sin\,\sin(\lambda_m x) \qquad \lambda_m = \frac{m\pi}{a} \tag{37}$$

The function Ψ_n may be attained by substituting x, m and a, respectively by y, n and b. Setting the coefficient matrix for the abovementioned results in the eigenvalue mentioned below issue

$$([K] + \omega^2[M])\begin{Bmatrix} W_b \\ W_s \end{Bmatrix} = 0 \tag{38}$$

whereby [M] as well as [K] are the mass matrix and stiffness matrix, respectively. Lastly, putting the coefficient matrix to zero provides the natural frequencies. Notably, the calculations presented are reliant on the dimensionless quantities as follows

$$\widehat{\omega} = \omega\frac{a^2}{h}\sqrt{\frac{\rho}{E}}, \quad K_w = k_w\frac{a^4}{D^*}, \quad K_p = k_p\frac{a^2}{D^*} \\ D^* = \frac{Eh^3}{12(1-\nu^2)}, \quad \mu = \frac{ea}{a}, \quad \lambda = \frac{l}{a} \tag{39}$$

4. Numerical results and discussions

This segment has been allocated to analyze the vibration tendencies for the nonlocal strain gradient graphene sheet mass sensors on elastic substrates that are according to two-variable shear deformation theory. Consequently, the framework presents two scale coefficients pertaining to strain gradient as well as nonlocal effects in order to obtain an increasingly precise investigation of graphene sheets. Furthermore, the Graphene Sheets' material properties are: E = 1 TPa, ν = 0.19 and ρ = 2300 kg/m^3. Additionally, the breadth and length of the graphene sheet are regarded to be h = 0.34 nm, a = 10 nm. Figs. 1 and 2, respectively, provide a visualization as to the distribution of nanoparticles and the configuration of the graphene sheet. The graphene sheet's natural frequencies get checked to correspond alongside the ones procured by Sobhy (2016) for numerous nonlocal parameters (μ = 0, 1, 2, 3, 4 nm^2) as well as the foundation constants ({K_w, K_p} = {(0, 0), (100, 0), (0, 20)}. As counted in Table 1, the procured frequencies through employing the current Galerkin method are held to be in prime accordance with that of the precise solution introduced by Sobhy (2016). The length scale parameter or strain gradient has been fixed at zero (λ = 0) for the purposes of the comparative study.

Upon the vibration frequencies of graphene sheet mass

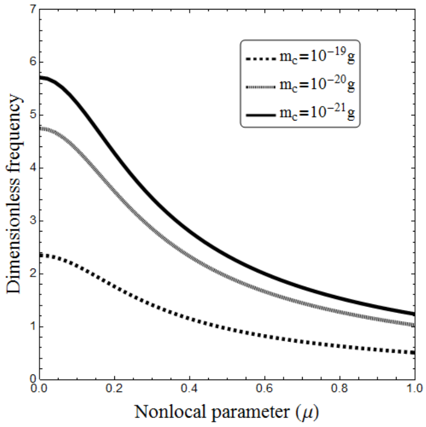

(a) Nonlocal (λ = 0)

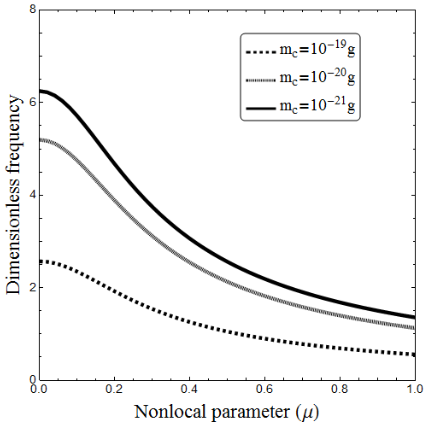

(b) Nonlocal strain gradient (λ = 0.1)

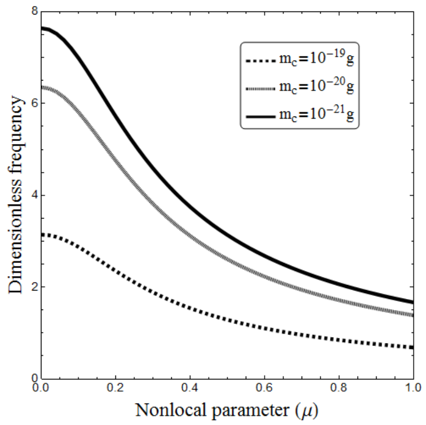

(c) Nonlocal strain gradient (λ = 0.2)

Fig. 3 Dimensionless frequency of graphene sheet against nonlocal parameter for various strain gradient parameters as well as nanoparticle mass ($\xi = 0.5,\ \eta = 0.5$)

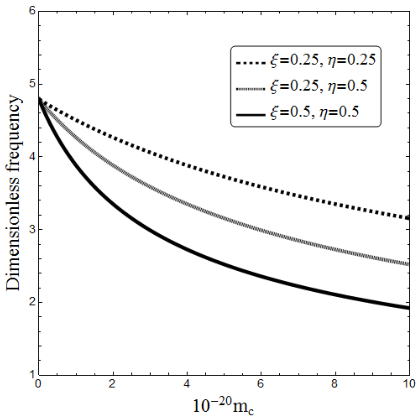

(a) K_w = 0, K_p = 0

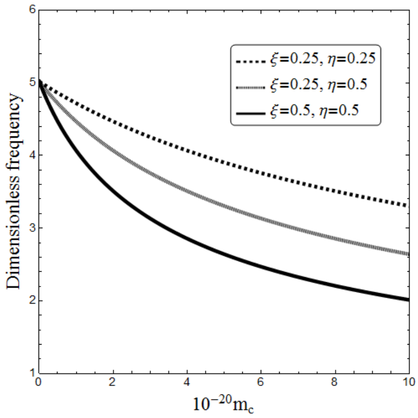

(b) K_w = 25, K_p = 0

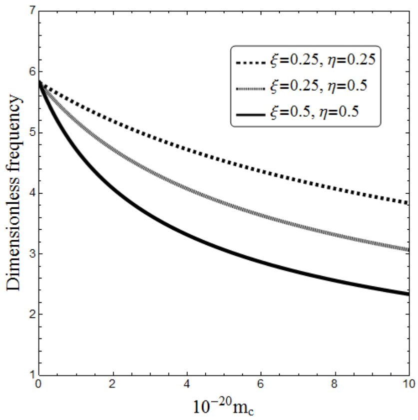

(c) K_w = 25, K_p = 5

Fig. 4 Dimensionless frequency of graphene sheet against nanoparticle mass for various foundation parameters as well as nanoparticle location (μ = 0.2, λ = 0.1)

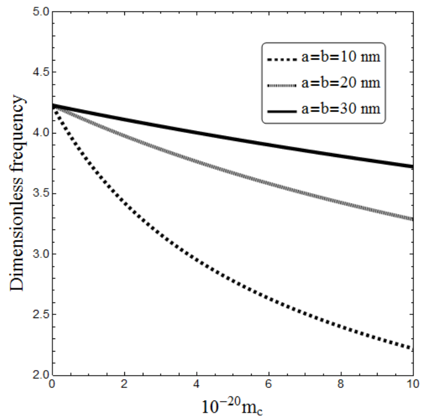

(a) a/b = 0.5

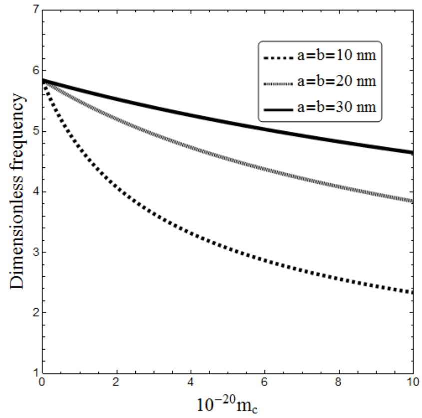

(b) a/b = 1

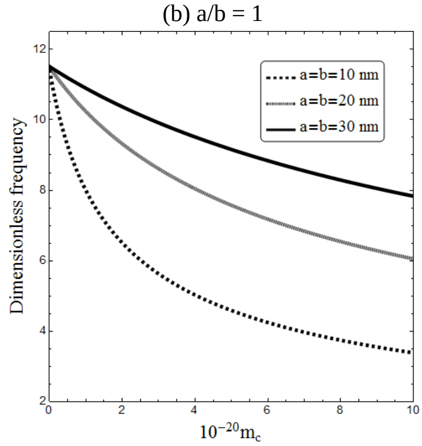

(c) a/b = 2

Fig. 5 Dimensionless frequency of graphene sheet against nanoparticle mass for various aspect ratios (μ = 0.2, λ = 0.1, K_w = 25, K_p = 5)

sensors, Fig. 3 presents an evaluation of the effects of nonlocal and strain gradient. The previously mentioned figure acknowledges a variety of values of the length scale (λ = 0, 0.1, 0.2) and nonlocal parameters (μ = 0~1). Upon λ = 0, it is evident that the natural frequencies of a graphene sheet according to proven nonlocal elasticity theory are capable of being acquired, nonetheless, upon both λ = 0 and μ = 0, the outcomes founded upon classical continuum mechanics get decreed. It has been noted how an augmentation of nonlocal parameters would result in a reduction in the graphene sheet's natural frequency and the record posits that the stiffness-softening effect exerted by a nonlocal parameter results in frequencies of a lower vibration. However, the nonlocal parameters impact upon the natural frequencies' magnitude is dependent on the valuation of the length scale parameter or strain gradient. As a matter of fact, an upsurge of the length scale parameter that accentuates the stiffness-hardening effect because of the strain gradients will cause an upsurge in the graphene sheet's natural frequency. Additionally, at set length scale and nonlocal parameters, an amelioration in the mass of the

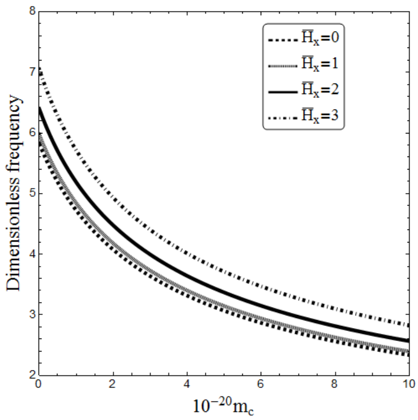

(a) μ = 0.2, λ = 0.1

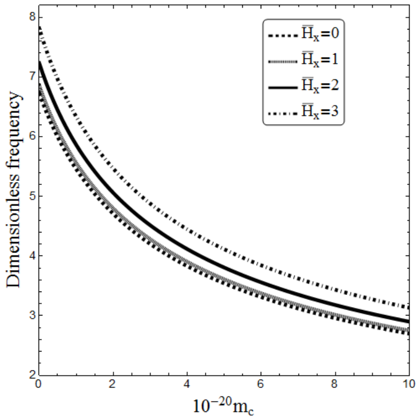

(b) μ = 0.2, λ = 0.2

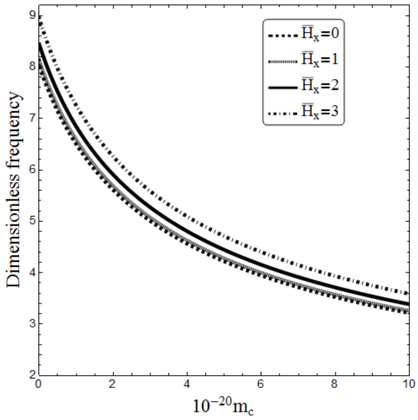

(c) μ = 0.2, λ = 0.3

Fig. 6 Dimensionless frequency of graphene sheet against nanoparticle mass for various magnetic field intensities (K_w = 25, K_p = 5)

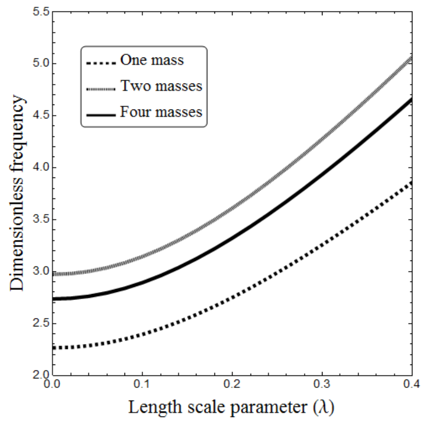

(a) $m_c = 10^{-19}g$

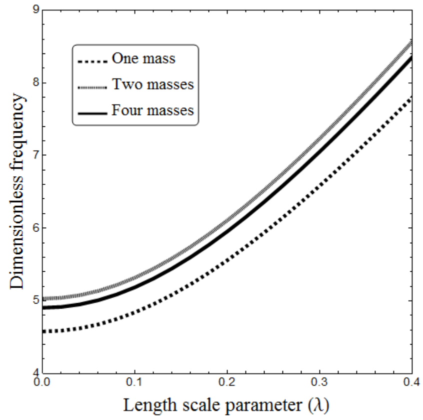

(b) $m_c = 10^{-20}g$

Fig. 7 Dimensionless frequency of graphene sheet against length scale parameter for various amount of nanoparticles (μ = 0.2, K_w = 25, K_p = 5, H_x = 1)

nanoparticle results in a reduction of the vibration frequencies. Moreover, it is noted that the impact of nonlocal parameters on the vibration frequency of nano-mechanical mass sensors is increasingly significant in regards to smaller nanoparticles.

Fig. 4 presents the variation of dimensionless frequency of graphene sheet against nanoparticle mass for numerous foundation parameters as well as nanoparticle location at μ = 0.2 and λ = 0.1. It has been discovered that an increase in mass results in a decrease in the vibration frequencies for every nanoparticle. Furthermore, one can observe the variability of frequency which is evident when the mass that is attached is greater than 10^{-21} g. Factually, the mass sensitivity of the nano-mechanical mass sensor is capable of recording at least 10^{-21} g. Also, it is noted how the impact of the location of nanoparticles is prominently enhanced upon an increase of the attached mass. Upon the closing of the nanoparticles proximity to the plate center, there is a reduction in the vibration frequency of the nano-mechanical mass sensor. As a result of that, it can be noticed how the vibration behavior for the nano-mechanical mass sensor relies on values from both the Pasternak and Winkler variables. In actuality, the Pasternak layer contains a lasting relationship with the sheet of graphene, while the Winkler layer contains a discontinued relationship with the graphene sheets. Adding to the parameters for Winkler and Pasternak results in greater frequencies through improving the graphene sheet's bending rigidity. Although, comparison with the Winkler layer, Pasternak layer displays more growing impact on frequencies.

Fig. 5 demonstrates the variant dimensionless frequencies compared to the attached mass pertaining to various length and width parameters as well as aspect ratios (a/b) at K_w = 25, K_p = 5, μ = 0.2, λ = 0.1. Notably, graphene sheets with greater lengths contain greater vibration frequencies. This is due to the fact that, graphene sheets with reduced sizes happen to be more rigid. Thus, a graphene sheet mass sensor with smaller sizes is much more sensitive with the attached mass. In fact, variation of dimensionless frequency with respects to the mass attached, becomes more significant as the size of graphene sheet reduces.

Magnetic field's impact on the vibrational frequency of the nano-mechanical mass sensor in related to the mass attached for different scale parameters is presented in Fig. 6 at K_w = 25, K_p = 5. It should be remembered how the graphene layer has a stiffness-hardening effect on the in-plane magnetic field. As a matter of fact, increased intensity of the magnetic field results in large frequencies. In conclusion, in-plane magnetic field plays a crucial role on the vibrational behavior of nano-mechanical mass sensor which must be planned to be checked in order to have and sustain their accurate design. While nano-mechanical mass sensor vibration behavior relies on the importance of the scale parameters. Subsequently, if $\mu > \lambda$, the nonlocal influence becomes more predominant, and if $\mu < \lambda$, the impact of the strain gradient is stronger, contributing to vibration frequency enlargement.

Fig. 7 shows the variety of alternative dimensionless frequency of graphene sheet as compared to the length scale parameter for numerous number of nanoparticles at μ = 0.2, K_w = 25, K_p = 5, H_x = 1. Another important note should be the overall mass of nanoparticles is 10^{-19} g and 10^{-20} g is considered as an assumption. The graphene sheet shows minimal frequency when one attached mass is positioned at the middle of the layer. Although, when two masses are attached at the location (ξ, η) = (0.25, 0.5), (0.75, 0.5), they give off larger frequencies as compared to both one attached mass along with four attached masses. Lastly, the location and effective mass have dominant effect on vibration techniques, due to the overall nanoparticle mass which is identical.

5. Conclusions

In order to explore the free vibration tendencies of single-layer graphene sheet mass sensors which rest upon an elastic medium through utilizing a refined two-variable plate theory, this composition has employed the theory of nonlocal strain gradient. Following the introduction of two scale parameters in order to acquire both stiffness-hardening alongside stiffness-softening influences that commensurate with strain gradient and nonlocal effects, Hamilton's principle is utilized to derive the principal equation of a nonlocal strain gradient graphene sheet. The aforementioned equations are elucidated through making use of Galerkin's technique in regards to obtaining the natural frequencies. The natural frequency of graphene sheets has accordingly been noted to be reduced following an increase of nonlocal parameters. Contrastingly, it has been observed that an upsurge of the length scale parameter which accentuates the stiffness-hardening effect as a result of the strain gradients corresponds with an upsurge of natural frequency. The mass and number of attached nanoparticles are regarded to impact all these observations. Nevertheless, upon proximity of the nanoparticle to the plate center, there is a reduction in the frequency of vibration for the nano-mechanical mass sensor.

Acknowledgments

The work was supported by the Deanship of Scientific Research at Prince Sattam Bin Abdulaziz University under the research project No 2016/01/6698.

References

Aksencer, T. and Aydogdu, M. (2011), "Levy type solution method for vibration and buckling of nanoplates using nonlocal elasticity theory", *Physica E Low Dimens. Syst. Nanostruct.*, **43**(4), 954-959. https://doi.org/10.1016/j.physe.2010.11.024.

Ansari, R. and Sahmani, S. (2013), "Prediction of biaxial buckling behavior of single-layered graphene sheets based on nonlocal plate models and molecular dynamics simulations", *Appl. Math. Model.*, **37**(12), 7338-7351. https://doi.org/10.1016/j.apm.2013.03.004.

Ansari, R., Arash, B. and Rouhi, H. (2011), "Vibration characteristics of embedded multi-layered graphene sheets with different boundary conditions via nonlocal elasticity", *Compos. Struct.*, **93**(9), 2419-2429. https://doi.org/10.1016/j.compstruct.2011.04.006.

Arabnejad Khanouki, M.M., Ramli Sulong, N.H. and Shariati, M. (2010), "Investigation of seismic behaviour of composite structures with concrete filled square steel tubular (CFSST) column by push-over and time-history analyses", *Proceedings of the 4th International Conference on Steel and Composite Structures*, Sydney, Australia, July.

Arabnejad Khanouki, M.M., Ramli Sulong, N.H. and Shariati, M. (2011), "Behavior of through beam connections composed of CFSST columns and steel beams by finite element studying", *Adv. Mater. Res.*, **168**, 2329-2333. http://dx.doi.org/10.4028/www.scientific.net/AMR.168-170.2329.

Arabnejad Khanouki, M.M., Ramli Sulong, N.H., Shariati, M. and Tahir, M.M. (2016), "Investigation of through beam connection to concrete filled circular steel tube (CFCST) column", *J. Constr. Steel Res.*, **121**, 144-162. https://doi.org/10.1016/j.jcsr.2016.01.002.

Arani, A.G., Haghparast, E. and Zarei, H.B. (2016), "Nonlocal vibration of axially moving graphene sheet resting on orthotropic visco-Pasternak foundation under longitudinal magnetic field", *Physica B Condens. Matter*, **495**, 35-49. https://doi.org/10.1016/j.physb.2016.04.039.

Armaghani, D.J., Mirzaei, F., Shariati, M., Trung, N.T., Shariati, M. and Trnavac, D. (2020), "Hybrid ANN-based techniques in predicting cohesion of sandy-soil combined with fiber", *Geomech. Eng., Int. J.*, **20**(3), 191-205. https://doi.org/10.12989/gae.2020.20.3.191.

Bessaim, A., Houari, M.S.A., Bernard, F. and Tounsi, A. (2015), "A nonlocal quasi-3D trigonometric plate model for free vibration behaviour of micro/nanoscale plates", *Struct. Eng. Mech., Int. J.*, **56**(2), 223-240. https://doi.org/10.12989/sem.2015.56.2.223.

Chen, C., Shi, L., Shariati, M., Toghroli, A., Mohamad, E.T., Bui, D.T. and Khorami, M. (2019), "Behavior of steel storage pallet racking connection-A review", *Steel Compos. Struct., Int. J.*, **30**(5), 457-469. https://doi.org/10.12989/scs.2019.30.5.457.

Daie, M., Jalali, A., Suhatril, M., Shariati, M., Arabnejad Khanouki, M.M., Shariati, A. and Kazemi-Arbat, P. (2011), "A new finite element investigation on pre-bent steel strips as damper for vibration control", *Int. J. Phys. Sci.*, **6**(36), 8044-8050. https://doi.org/10.5897/ijps11.1585.

Davoodnabi, S.M., Mirhosseini, S.M. and Shariati, M. (2019), "Behavior of steel-concrete composite beam using angle shear connectors at fire condition", *Steel Compos. Struct., Int. J.*, **30**(2), 141-147. https://doi.org/10.12989/scs.2019.30.2.141.

Ebrahimi, F. and Barati, M.R. (2016a), "Vibration analysis of nonlocal beams made of functionally graded material in thermal environment", *Eur. Phys. J. Plus*, **131**(8), 279. https://doi.org/10.1140/epjp/i2016-16279-y.

Ebrahimi, F. and Barati, M.R. (2016b), "A unified formulation for dynamic analysis of nonlocal heterogeneous nanobeams in hygro-thermal environment", *Appl. Phys. A*, **122**(9), 792. https://doi.org/10.1007/s00339-016-0322-2.

Ebrahimi, F. and Barati, M.R. (2016c), "A nonlocal higher-order refined magneto-electro-viscoelastic beam model for dynamic analysis of smart nanostructures", *Int. J. Eng. Sci.*, **107**, 183-196. https://doi.org/10.1016/j.ijengsci.2016.08.001.

Ebrahimi, F. and Barati, M.R. (2016d), "Hygrothermal buckling analysis of magnetically actuated embedded higher order functionally graded nanoscale beams considering the neutral surface position", *J. Therm. Stress*, **39**(10), 1210-1229. https://doi.org/10.1080/01495739.2016.1215726.

Ebrahimi, F. and Barati, M.R. (2016e), "Vibration analysis of smart piezoelectrically actuated nanobeams subjected to magneto-electrical field in thermal environment", *J. Vib. Control*, **24**(3), 549-564. https://doi.org/10.1177/1077546316646239.

Ebrahimi, F. and Barati, M.R. (2016f), "Static stability analysis of smart magneto-electro-elastic heterogeneous nanoplates embedded in an elastic medium based on a four-variable refined plate theory", *Smart Mater. Struct.*, **25**(10), 105014. https://doi.org/10.1088/0964-1726/25/10/105014.

Ebrahimi, F. and Barati, M.R. (2016g), "Wave propagation analysis of quasi-3D FG nanobeams in thermal environment based on nonlocal strain gradient theory", *Appl. Phys. A*, **122**(9), 843. https://doi.org/10.1007/s00339-016-0368-1.

Ebrahimi, F. and Barati, M.R. (2016h), "Size-dependent dynamic modeling of inhomogeneous curved nanobeams embedded in elastic medium based on nonlocal strain gradient theory", *Proc. Inst. Mech. Eng. C J. Mech. Eng. Sci.*, **231**(23), 4457-4469. https://doi.org/10.1177/0954406216668912.

Ebrahimi, F. and Barati, M.R. (2017a), "Hygrothermal effects on vibration characteristics of viscoelastic FG nanobeams based on nonlocal strain gradient theory", *Compos. Struct.*, **159**, 433-444. https://doi.org/10.1016/j.compstruct.2016.09.092.

Ebrahimi, F. and Barati, M.R. (2017b), "A nonlocal strain gradient refined beam model for buckling analysis of size-dependent shear-deformable curved FG nanobeams", *Compos. Struct.*, **159**, 174-182. https://doi.org/10.1016/j.compstruct.2016.09.058.

Ebrahimi, F. and Salari, E. (2015), "Thermo-mechanical vibration analysis of a single-walled carbon nanotube embedded in an elastic medium based on higher-order shear deformation beam theory", *J. Mech. Sci. Technol.*, **29**(9), 3797-3803. https://doi.org/10.1007/s12206-015-0826-2.

Ebrahimi, F. and Shafiei, N. (2016), "Influence of initial shear stress on the vibration behavior of single-layered graphene sheets embedded in an elastic medium based on Reddy's higher-order shear deformation plate theory", *Mech. Adv. Mater. Struct.*, **24**(9), 761-772. https://doi.org/10.1080/15376494.2016.1196781.

Ebrahimi, F., Barati, M.R. and Dabbagh, A. (2016), "A nonlocal strain gradient theory for wave propagation analysis in temperature-dependent inhomogeneous nanoplates", *Int. J. Eng. Sci.*, **107**, 169-182. https://doi.org/10.1016/j.ijengsci.2016.07.008.

Ebrahimi, F., Karimiasl, M. and Mahesh, V. (2019), "Chaotic dynamics and forced harmonic vibration analysis of magneto-electro-viscoelastic multiscale composite nanobeam", *Eng. Comput.*, **2019**, 1-14. https://doi.org/10.1007/s00366-019-00865-3.

Eringen, A.C. (1983), "On differential equations of nonlocal elasticity and solutions of screw dislocation and surface waves", *J. Appl. Phys.*, **54**(9), 4703-4710. https://doi.org/10.1063/1.332803.

Eringen, A.C. and Edelen, D.G.B. (1972), "On nonlocal elasticity", *Int. J. Eng. Sci.*, **10**(3), 233-248. https://doi.org/10.1016/0020-7225(72)90039-0.

Farajpour, A., Shahidi, A.R., Mohammadi, M. and Mahzoon, M. (2012), "Buckling of orthotropic micro/nanoscale plates under linearly varying in-plane load via nonlocal continuum mechanics", *Compos. Struct.*, **94**(5), 1605-1615. https://doi.org/10.1016/j.compstruct.2011.12.032.

Georgantzinos, S.K. (2017), "A new finite element for an efficient mechanical analysis of graphene structures using computer aided design/computer aided engineering techniques", *J. Comput. Theor. Nanosci.*, **14**, 5347-5354. https://doi.org/10.1166/jctn.2017.6949.

Georgantzinos, S.K., Giannopoulos, G.I. and Anifantis, N.K. (2016), "Coupled thermomechanical behavior of graphene using the spring- based finite element approach", *J. Appl. Phys.*, **120**(1), 014305. https://doi.org/10.1063/1.4957289.

Hamidian, M., Shariati, M., Arabnejad, M. and Sinaei, H. (2011), "Assessment of high strength and light weight aggregate concrete properties using ultrasonic pulse velocity technique", *Int. J. Phys. Sci.*, **6**(22), 5261-5266. https://doi.org/10.5897/IJPS11.1081.

Hashemi, S.H., Mehrabani, H. and Ahmadi-Savadkoohi, A. (2015), "Exact solution for free vibration of coupled double viscoelastic graphene sheets by viscoPasternak medium", *Compos. Part B Eng.*, **78**, 377-383. https://doi.org/10.1016/j.compositesb.2015.04.008.

Heydari, A. and Shariati, M. (2018), "Buckling analysis of tapered BDFGM nano-beam under variable axial compression resting on elastic medium", *Struct. Eng. Mech., Int. J.*, **66**(6), 737-748. https://doi.org/10.12989/sem.2018.66.6.737.

Hosseinpour, E., Baharom, S., Badaruzzaman, W.H.W., Shariati, M. and Jalali, A. (2018), "Direct shear behavior of concrete filled hollow steel tube shear connector for slim-floor steel beams", *Steel Compos. Struct., Int. J.*, **26**(4), 485-499. https://doi.org/10.12989/scs.2018.26.4.485.

Ismail, M., Shariati, M., Awal, A.A., Chiong, C.E., Chahnasir, E.S, Porbar, A., Heydari, A. and Khorami, M. (2018), "Strengthening of bolted shear joints in industrialized ferrocement construction", *Steel Compos. Struct., Int. J.*, **28**(6), 681-690. https://doi.org/10.12989/scs.2018.28.6.681.

Jalali, A., Daie, M., Nazhadan, S.V.M., Kazemi-Arbat, P. and Shariati, M. (2012), "Seismic performance of structures with pre-bent strips as a damper", *Int. J. Phys. Sci.*, **7**(26), 4061-4072. https://doi.org/10.5897/IJPS11.1324.

Jiang, R.W., Shen, Z.B. and Tang, G.J. (2016), "Vibration analysis of a single-layered graphene sheet-based mass sensor using the Galerkin strip distributed transfer function method", *Acta Mech.*, **227**(10), 2899-2910. https://doi.org/10.1007/s00707-016-1649-7.

Katebi, J., Shoaei-parchin, M., Shariati, M., Trung, N.T. and Khorami, M. (2019), "Developed comparative analysis of metaheuristic optimization algorithms for optimal active control of structures", *Eng. Comput.*, **36**, 1539-1558. https://doi.org/10.1007/s00366-019-00780-7.

Khorami, M., Alvansazyazdi, M., Shariati, M., Zandi, Y., Jalali, A. and Tahir, M. (2017a), "Seismic performance evaluation of buckling restrained braced frames (BRBF) using incremental nonlinear dynamic analysis method (IDA)", *Earthq. Struct., Int.*

J., **13**(6), 531-538.
http://dx.doi.org/10.12989/eas.2017.13.6.531.

Khorami, M., Khorami, M., Motahar, H., Alvansazyazdi, M., Shariati, M., Jalali, A. and Tahir, M.M. (2017b), "Evaluation of the seismic performance of special moment frames using incremental nonlinear dynamic analysis", *Struct*. *Eng*. *Mech*., *Int*. *J*., **63**(2), 259-268.
https://doi.org/10.12989/sem.2017.63.2.259.

Khorramian, K., Maleki, S., Shariati, M. and Ramli Sulong, N.H. (2016), "Behavior of tilted angle shear connectors", *PLoS One*, **10**(12), e0144288. https://doi.org/10.1371/journal.pone.0144288.

Khorramian, K., Maleki, S., Shariati, M., Jalali, A. and Tahir, M. (2017), "Numerical analysis of tilted angle shear connectors in steel-concrete composite systems", *Steel Compos*. *Struct*., *Int*. *J*., **23**(1), 67-85. https://doi.org/10.12989/scs.2017.23.1.067.

Lam, D.C.C., Yang, F., Chong, A.C.M., Wang, J. and Tong, P. (2003), "Experiments and theory in strain gradient elasticity", *J*. *Mech*. *Phys*. *Solids*, **51**(8), 1477-1508.
https://doi.org/10.1016/S0022-5096(03)00053-X.

Li, L. and Hu, Y. (2016), "Wave propagation in fluid-conveying viscoelastic carbon nanotubes based on nonlocal strain gradient theory", *Comput*. *Mater*. *Sci*., **112**, 282-288.
https://doi.org/10.1016/j.commatsci.2015.10.044.

Li, L., Hu, Y. and Li, X. (2016), "Longitudinal vibration of size-dependent rods via nonlocal strain gradient theory", *Int*. *J*. *Mech*. *Sci*., **115**, 135-144.
https://doi.org/10.1016/j.ijmecsci.2016.06.011.

Li, D., Toghroli, A., Shariati, M., Sajedi, F., Bui, D.T., Kianmehr, P., Mohamad, E.T. and Khorami, M. (2019), "Application of polymer, silica-fume and crushed rubber in the production of Pervious concrete", *Smart Struct*. *Syst*., *Int*. *J*., **23**(2), 207-214.
https://doi.org/10.12989/sss.2019.23.2.207.

Lim, C.W., Zhang, G. and Reddy, J.N. (2015), "A higher-order nonlocal elasticity and strain gradient theory and its applications in wave propagation", *J*. *Mech*. *Phys*. *Solids*, **78**, 298-313.
https://doi.org/10.1016/j.jmps.2015.02.001.

Luo, Z., Sinaei, H., Ibrahim, Z., Shariati, M., Jumaat, Z., Wakil, K., Pham, B.T., Mohamad, E.T. and Khorami, M. (2019), "Computational and experimental analysis of beam to column joints reinforced with CFRP plates", *Steel Compos*. *Struct*., *Int*. *J*., **30**(3), 271-280. http://dx.doi.org/10.12989/scs.2019.30.3.271.

Mansouri, I., Safa, M., Ibrahim, Z., Kisi, O., Tahir, M.M., Baharom, S.B. and Azimi, M. (2016), "Strength prediction of rotary brace damper using MLR and MARS", *Struct*. *Eng*. *Mech*., *Int*. *J*., **60**(3), 471-488.
https://doi.org/10.12989/sem.2016.60.3.471.

Mansouri, I., Shariati, M., Safa, M., Ibrahim, Z., Tahir, M. and Petković, D. (2019), "Analysis of influential factors for predicting the shear strength of a V-shaped angle shear connector in composite beams using an adaptive neuro-fuzzy technique", *J*. *Intell*. *Manuf*., **30**(3), 1247-1257.
https://doi.org/10.1007/s10845-017-1306-6.

Milovancevic, M., Marinović, J.S., Nikolić, J., Kitić, A., Shariati, M., Trung, N.T., Wakil, K. and Khorami, M. (2019), "UML diagrams for dynamical monitoring of rail vehicles", *Physica A*, **531**, 121169. https://doi.org/10.1016/j.physa.2019.121169.

Mohammadhassani, M., Nezamabadi-Pour, H., Suhatril, M. and Shariati, M. (2013), "Identification of a suitable ANN architecture in predicting strain in tie section of concrete deep beams", *Struct*. *Eng*. *Mech*., *Int*. *J*., **46**(6), 853-868.
https://doi.org/10.12989/sem.2013.46.6.853.

Mohammadhassani, M., Akib, S., Shariati, M., Suhatril, M. and Arabnejad Khanouki, M.M. (2014a), "An experimental study on the failure modes of high strength concrete beams with particular references to variation of the tensile reinforcement ratio", *Eng*. *Fail*. *Anal*., **41**, 73-80.
https://doi.org/10.1016/j.engfailanal.2013.08.014.

Mohammadhassani, M., Nezamabadi-Pour, H., Suhatril, M. and Shariati, M. (2014b), "An evolutionary fuzzy modelling approach and comparison of different methods for shear strength prediction of high-strength concrete beams without stirrups", *Smart Struct*. *Syst*., *Int*. *J*., **14**(5), 785-809.
http://dx.doi.org/10.12989/sss.2014.14.5.785.

Mohammadhassani, M., Suhatril, M., Shariati, M. and Ghanbari, F. (2014c), "Ductility and strength assessment of HSC beams with varying of tensile reinforcement ratios", *Struct*. *Eng*. *Mech*., *Int*. *J*., **48**(6), 833-848.
https://doi.org/10.12989/sem.2013.48.6.833.

Mohammadhassani, M., Saleh, A., Suhatril, M. and Safa, M. (2015), "Fuzzy modelling approach for shear strength prediction of RC deep beams", *Smart Struct*. *Syst*., *Int*. *J*., **16**(3), 497-519.
https://doi.org/10.12989/sss.2015.16.3.497.

Mohammadi, M., Goodarzi, M., Ghayour, M. and Farajpour, A. (2013), "Influence of in-plane pre-load on the vibration frequency of circular graphene sheet via nonlocal continuum theory", *Compos*. *Part B Eng*., **51**, 121-129.
https://doi.org/10.1016/j.compositesb.2013.02.044.

Mohammadi, M., Farajpour, A., Moradi, A. and Ghayour, M. (2014), "Shear buckling of orthotropic rectangular graphene sheet embedded in an elastic medium in thermal environment", *Compos*. *Part B Eng*., **56**, 629-637.
https://doi.org/10.1016/j.compositesb.2013.08.060.

Mortazavi, B., Rémond, Y., Ahzi, S. and Toniazzo, V. (2012), "Thickness and chirality effects on tensile behavior of few-layer graphene by molecular dynamics simulations", *Comput*. *Mater*. *Sci*., **53**(1), 298-302.
https://doi.org/10.1016/j.commatsci.2011.08.018.

Murmu, T., McCarthy, M.A. and Adhikari, S. (2013), "In-plane magnetic field affected transverse vibration of embedded single-layer graphene sheets using equivalent nonlocal elasticity approach", *Compos*. *Struct*., **96**, 57-63.
https://doi.org/10.1016/j.compstruct.2012.09.005.

Naghipour, M., Niak, K.M., Shariati, M. and Toghroli, A. (2020a), "Effect of progressive shear punch of a foundation on a reinforced concrete building behavior", *Steel Compos*. *Struct*., *Int*. *J*., **35**(2), 279-294.
https://doi.org/10.12989/scs.2020.35.2.279.

Naghipour, M., Yousofizinsaz, G. and Shariati, M. (2020b), "Experimental study on axial compressive behavior of welded built-up CFT stub columns made by cold-formed sections with different welding lines", *Steel Compos*. *Struct*., *Int*. *J*., **34**(3), 347-359. https://doi.org/10.12989/scs.2020.34.3.347.

Narendar, S. and Gopalakrishnan, S. (2012), "Scale effects on buckling analysis of orthotropic nanoplates based on nonlocal two-variable refined plate theory", *Acta Mech*., **223**(2), 395-413. https://doi.org/10.1007/s00707-011-0560-5.

Nasrollahi, S., Maleki, S., Shariati, M., Marto, A. and Khorami, M. (2018), "Investigation of pipe shear connectors using push out test." *Steel Compos*. *Struct*., *Int*. *J*., **27**(5), 537-543.
http://dx.doi.org/10.12989/scs.2018.27.5.537.

Nosrati, A., Zandi, Y., Shariati, M., Khademi, K., Darvishnezhad Aliabad, M., Marto, A., Mu'azu, M., Ghanbari, E., Mandizadeh, M.B. and Shariati, A. (2018), "Portland cement structure and its major oxides and fineness", *Smart Struct*. *Syst*., *Int*. *J*., **22**(4), 425-432. https://doi.org/10.12989/sss.2018.22.4.425.

Obhy, M. (2014), "Thermomechanical bending and free vibration of single-layered graphene sheets embedded in an elastic medium", *Physica E Low Dimens*. *Syst*. *Nanostruct*., **56**, 400-409. https://doi.org/10.1016/j.physe.2013.10.017.

Paknahad, M., Shariati, M., Sedghi, Y., Bazzaz, M. and Khorami, M. (2018), "Shear capacity equation for channel shear connectors in steel-concrete composite beams", *Steel Compos*. *Struct*., *Int*. *J*., **28**(4), 483-494.
https://doi.org/10.12989/scs.2018.28.4.483.

Pradhan, S.C. and Kumar, A. (2011), "Vibration analysis of orthotropic graphene sheets using nonlocal elasticity theory and differential quadrature method", *Compos. Struct.*, **93**(2), 774-779. https://doi.org/10.1016/j.compstruct.2010.08.004.

Pradhan, S.C. and Murmu, T. (2009), "Small scale effect on the buckling of single-layered graphene sheets under biaxial compression via nonlocal continuum mechanics", *Comput. Mater. Sci.*, **47**(1), 268-274. https://doi.org/10.1016/j.commatsci.2009.08.001.

Qi, C.C. (2020), "Big data management in the mining industry", *Int. J. Min. Metall. Mater.*, **27**(2), 131-139. https://doi.org/10.1007/s12613-019-1937-z.

Razavian, L., Naghipour, M., Shariati, M. and Safa, M. (2020), "Experimental study of the behavior of composite timber columns confined with hollow rectangular steel sections under compression", *Struct. Eng. Mech., Int. J.*, **74**(1), 145-156. https://doi.org/10.12989/sem.2020.74.1.145.

Sadeghi Chahnasir, E, Zandi, Y., Shariati, M., Dehghani, E., Toghroli, A., Mohamed, E.T., Shariati, A., Safa, M., Wakil, K. and Khorami, M. (2018), "Application of support vector machine with firefly algorithm for investigation of the factors affecting the shear strength of angle shear connectors", *Smart Struct. Syst., Int. J.*, **22**(4), 413-424. http://dx.doi.org/10.12989/sss.2018.22.4.413.

Safa, M., Shariati, M., Ibrahim, Z., Toghroli, A., Baharom, S.B., Nor, N.M. and Petkovic, D. (2016), "Potential of adaptive neuro fuzzy inference system for evaluating the factors affecting steel-concrete composite beam's shear strength", *Steel Compos. Struct., Int. J.*, **21**(3), 679-688. https://doi.org/10.12989/scs.2016.21.3.679.

Safa, M., Maleka, A., Arjomand, M.A., Khorami, M. and Shariati, M. (2019), "Strain rate effects on soil-geosynthetic interaction in fine-grained soil", *Geomech. Eng., Int. J.*, **19**(6), 533-542. https://doi.org/10.12989/gae.2019.19.6.533.

Safa, M., Sari, P.A., Shariati, M., Suhatril, M., Trung, N.T., Wakil, K. and Khorami, M. (2020), "Development of neuro-fuzzy and neuro-bee predictive models for prediction of the safety factor of eco-protection slopes", *Physica A*, **550**, 124046. https://doi.org/10.1016/j.physa.2019.124046.

Sajedi, F. and Shariati, M. (2019), "Behavior study of NC and HSC RCCs confined by GRP casing and CFRP wrapping", *Steel Compos. Struct., Int. J.*, **30**(5), 417-432. https://doi.org/10.12989/scs.2019.30.5.417.

Sari, P.A., Suhatril, M., Osman, N., Mu'azu, M., Dehghani, H., Sedghi, Y., Safa, M., Hasanipanah, M., Wakil, K. and Khorami, M. (2018), "An intelligent based-model role to simulate the factor of safe slope by support vector regression", *Eng. Comput.*, **35**(4), 1521-1531. https://doi.org/10.1007/s00366-018-0677-4.

Sedghi, Y., Zandi, Y., Shariati, M., Ahmadi, E., Azar, V.M., Toghroli, A., Safa, M., Mohamad, E.T., Khorami, M. and Wakil, K. (2018). "Application of ANFIS technique on performance of C and L shaped angle shear connectors", *Smart Struct. Syst., Int. J.*, **22**(3), 335-340. https://doi.org/10.12989/sss.2018.22.3.335.

Shah, S., Sulong, N.H.R., Shariati, M. and Jumaat, M.Z. (2015), "Steel rack connections: Identification of most influential factors and a comparison of stiffness design methods", *PloS One*, **10**(10), e0139422. https://doi.org/10.1371/journal.pone.0139422.

Shah, S., Sulong, N.H.R., Shariati, M., Khan, R. and Jumaat, M. (2016a), "Behavior of steel pallet rack beam-to-column connections at elevated temperatures", *Thin-Wall. Struct.*, **106**, 471-483. https://doi.org/10.1016/j.tws.2016.05.021.

Shah, S., Sulong, N.H.R., Jumaat, M. and Shariati, M. (2016b), "State-of-the-art review on the design and performance of steel pallet rack connections", *Eng. Fail. Anal.*, **66**, 240-258. https://doi.org/10.1016/j.engfailanal.2016.04.017.

Shah, S., Sulong, N.H.R., Khan, R., Jumaat, M. and Shariati, M. (2016c), "Behavior of industrial steel rack connections", *Mech. Syst. Signal Process*, **70**, 725-740. https://doi.org/10.1016/j.ymssp.2015.08.026.

Shahabi, S., Sulong, N.H.R., Shariati, M., Mohammadhassani, M. and Shah, S. (2016a), "Numerical analysis of channel connectors under fire and a comparison of performance with different types of shear connectors subjected to fire", *Steel Compos. Struct., Int. J.*, **20**(3), 651-669. https://10.12989/scs.2016.20.3.651.

Shahabi, S., Sulong, N.H.R., Shariati, M. and Shah, S. (2016b), "Performance of shear connectors at elevated temperatures-A review", *Steel Compos. Struct., Int. J.*, **20**(1), 185-203. https://doi.org/10.12989/scs.2016.20.1.185.

Shariat, M., Shariati, M., Madadi, A. and Wakil, K. (2018), "Computational Lagrangian Multiplier Method by using for optimization and sensitivity analysis of rectangular reinforced concrete beams", *Steel Compos. Struct., Int. J.*, **29**(2), 243-256. https://doi.org/10.12989/scs.2018.29.2.243.

Shariati, M. (2013), "Behaviour of c-shaped shear connectors in stell concrete composite beams", Ph.D. Dissertation, Universiti Malaya, Kuala Lumpur, Malaysia.

Shariati, A. (2014), "Behaviour of c-shaped angle shear connectors in high strength concrete", M.Sc. Dissertation, Universiti Malaya, Kuala Lumpur, Malaysia.

Shariati, M. (2020), "Evaluation of seismic performance factors for tension-only braced frames", *Steel Compos. Struct., Int. J.*, **35**(4), 599-609. https://doi.org/10.12989/scs.2020.35.4.599.

Shariati, M., Ramli Sulong, N.H., and Arabnejad Khanouki, M.M. (2010), "Experimental and analytical study on channel shear connectors in light weight aggregate concrete", *Proceedings of the 4th International Conference on Steel & Composite Structures*, Sydney, Australia, July.

Shariati, M., Ramli Sulong, N.H., Arabnejad Khanouki, M.M. and Mahoutian, M. (2011a), "Shear resistance of channel shear connectors in plain, reinforced and lightweight concrete", *Sci. Res. Essays*, **6**(4), 977-983. https://doi.org/10.5897/SRE10.1120.

Shariati, M., Ramli Sulong, N.H., Arabnejad Khanouki, M.M., Shafigh, P. and Sinaei, H. (2011b), "Assessing the strength of reinforced concrete structures through ultrasonic pulse velocity and schmidt rebound hammer tests", *Sci. Res. Essays*, **6**(1), 213-220. https://doi.org/10.5897/SRE10.879.

Shariati, M., Ramli Sulong, N.H., Arabnejad Khanouki, M.M. and Shariati, A. (2011c), "Experimental and numerical investigations of channel shear connectors in high strength concrete", *Proceedings of the 2011 World Congress on Advances in Structural Engineering and Mechanics*, Seoul, Korea, August.

Shariati, M., Ramli Sulong, N.H., Sinaei, H., Arabnejad Khanouki, M.M. and Shafigh, P. (2011d), "Behavior of channel shear connectors in normal and light weight aggregate concrete (experimental and analytical study)", *Adv. Mater. Res.*, **168**, 2303-2307. https://doi.org/10.4028/www.scientific.net/AMR.168-170.2303.

Shariati, A., Sulong, N.H.R., Suhatril, M. and Shariati, M. (2012a), "Investigation of channel shear connectors for composite concrete and steel T-beam", *Int. J. Phys. Sci.*, **7**(11), 1828-1831. https://doi.org/10.5897/IJPS11.1604.

Shariati, A., Sulong, N.H.R., Suhatril, M. and Shariati, M. (2012b), "Various types of shear connectors in composite structures: A review", *Int. J. Phys. Sci.*, **7**(22), 2876-2890. https://doi.org/10.5897/IJPSx11.004.

Shariati, M., Ramli Sulong, N.H. and Arabnejad Khanouki, M.M. (2012c), "Experimental assessment of channel shear connectors under monotonic and fully reversed cyclic loading in high strength concrete", *Mater. Des.*, **34**, 325-331. https://doi.org/10.1016/j.matdes.2011.08.008.

Shariati, M., Ramli Sulong, N.H., Suhatril, M., Shariati, A., Arabnejad Khanouki, M.M. and Sinaei, H. (2012d), "Behaviour of c-shaped angle shear connectors under monotonic and fully reversed cyclic loading: An experimental study", *Mater. Des.*, **41**, 67-73. https://doi.org/10.1016/j.matdes.2012.04.039.

Shariati, M., Ramli Sulong, N.H., Suhatril, M., Shariati, A., Arabnejad Khanouki, M.M. and Sinaei, H. (2012e), "Fatigue energy dissipation and failure analysis of channel shear connector embedded in the lightweight aggregate concrete in composite bridge girders", *Proceedings of the Fifth International Conference on Engineering Failure Analysis*, Hague, Netherlands, July.

Shariati, M., Ramli Sulong, N.H., Suhatril, M., Shariati, A., Arabnejad Khanouki, M.M. and Sinaei, H. (2013), "Comparison of behaviour between channel and angle shear connectors under monotonic and fully reversed cyclic loading", *Constr. Build. Mater.*, **38**, 582-593. https://doi.org/10.1016/j.conbuildmat.2012.07.050.

Shariati, M., Shariati, A., Ramli Sulong, N.H., Suhatril, M. and Arabnejad Khanouki, M.M. (2014), "Fatigue energy dissipation and failure analysis of angle shear connectors embedded in high strength concrete", *Eng. Fail. Anal.*, **41**, 124-134. https://doi.org/10.1016/j.engfailanal.2014.02.017.

Shariati, M., Ramli Sulong, N.H., Shariati, A. and Arabnejad Khanouki, M.M. (2015), "Behavior of v-shaped angle shear connectors: experimental and parametric study", *Mater. Struct.*, **49**(9), 3909-3926. https://doi.org/10.1617/s11527-015-0762-8.

Shariati, M., Ramli Sulong, N.H., Shariati, A. and Kueh, A.B.H. (2016), "Comparative performance of channel and angle shear connectors in high strength concrete composites: An experimental study", *Constr. Build. Mater.*, **120**, 382-392. https://doi.org/10.1016/j.conbuildmat.2016.05.102.

Shariati, M., Toghroli, A., Jalali, A. and Ibrahim, Z. (2017), "Assessment of stiffened angle shear connector under monotonic and fully reversed cyclic loading", *Proceedings of the Fifth International Conference on Advances in Civil, Structural and Mechanical Engineering*, Bangkok, Thailand, August. https://doi.org/10.15224/978-1-63248-132-0-44.

Shariati, M., Tahir, M.M., Wee, T.C., Shah, S., Jalali, A., Abdullahi, M.A.M. and Khorami, M. (2018), "Experimental investigations on monotonic and cyclic behavior of steel pallet rack connections", *Eng. Fail. Anal.*, **85**, 149-166. https://doi.org/10.1016/j.engfailanal.2017.08.014.

Shariati, M., Azar, S.M., Arjomand, M.A., Tehrani, H.S., Daei, M. and Safa, M. (2019a), "Comparison of dynamic behavior of shallow foundations based on pile and geosynthetic materials in fine-grained clayey soils", *Geomech. Eng., Int. J.*, **19**(6), 473-484. https://doi.org/10.12989/gae.2019.19.6.473.

Shariati, M., Faegh, S.S., Mehrabi, P., Bahavarnia, S., Zandi, Y., Masoom, D.R., Toghroli, A., Trung, N.T. and Salih, M.N. (2019b), "Numerical study on the structural performance of corrugated low yield point steel plate shear walls with circular openings", *Steel Compos. Struct., Int. J.*, **33**(4), 569-581. https://doi.org/10.12989/scs.2019.33.4.569.

Shariati, M., Heyrati, A., Zandi, Y., Laka, H., Toghroli, A., Kianmehr, P., Safa, M., Salih, M.N. and Poi-Ngian, S. (2019c), "Application of waste tire rubber aggregate in porous concrete", *Smart Struct. Syst., Int. J.*, **24**(4), 553-566. https://doi.org/10.12989/sss.2019.24.4.553.

Shariati, M., Mafipour, M.S., Mehrabi, P., Bahadori, A., Zandi, Y., Salih, M.N., Nguyen, H., Dou, J., Song, X. and Poi-Ngian, S. (2019d), "Application of a hybrid artificial neural network-particle swarm optimization (ANN-PSO) model in behavior prediction of channel shear connectors embedded in normal and high-strength concrete", *Appl. Sci.*, **9**(24), 5534. https://doi.org/10.3390/app9245534.

Shariati, M., Mafipour, M.S., Mehrabi, P., Zandi, Y., Dehghani, D., Bahadori, A., Shariati, A., Trung, N.T., Salih, M.N. and Poi-Ngian, S. (2019e), "Application of extreme learning machine (ELM) and genetic programming (GP) to design steel-concrete composite floor systems at elevated temperatures", *Steel Compos. Struct., Int. J.*, **33**(3), 319-332. https://doi.org/10.12989/scs.2019.33.3.319.

Shariati, M., Rafiei, S., Zandi, Y., Fooladvand, R., Gharehaghaj, B., Shariat, A., Trung, N.T., Salih, M.N., Mehrabi, P. and Poi-Ngian, S. (2019f), "Experimental investigation on the effect of cementitious materials on fresh and mechanical properties of self-consolidating concrete", *Adv. Concrete Constr., Int. J.*, **8**(3), 225-237. https://doi.org/10.12989/acc.2019.8.3.225.

Shariati, M., Trung, N.T., Wakil, K., Mehrabi, P., Safa, M. and Khorami, M. (2019g), "Moment-rotation estimation of steel rack connection using extreme learning machine", *Steel Compos. Struct., Int. J.*, **31**(5), 427-435. https://doi.org/10.12989/scs.2019.31.5.427.

Shariati, M., Azar, S.M., Arjomand, M.A., Tehrani, H.S., Daei, M. and Safa, M. (2020a), "Evaluating the impacts of using piles and geosynthetics in reducing the settlement of fine-grained soils under static load", *Geomech. Eng., Int. J.*, **20**(2), 87-101. https://doi.org/10.12989/gae.2020.20.2.087.

Shariati, M., Ghorbani, M., Naghipour, M., Alinejad, N. and Toghroli, A. (2020b), "The effect of RBS connection on energy absorption in tall buildings with braced tube frame system", *Steel Compos. Struct., Int. J.*, **34**(3), 393-407. https://doi.org/10.12989/scs.2020.34.3.393.

Shariati, M., Mafipour, M.S., Ghahremani, B., Azarhomayun, F., Ahmadi, M., Trung, N.T. and Shariati, A. (2020c), "A novel hybrid extreme learning machine–grey wolf optimizer (ELM-GWO) model to predict compressive strength of concrete with partial replacements for cement", *Eng. Comput.*, **2020**, 1-23. https://doi.org/10.1007/s00366-020-01081-0.

Shariati, M., Mafipour, M.S., Haido, J.H., Yousif, S.T., Toghroli, A., Trung, N.T. and Shariati, A. (2020d), "Identification of the most influencing parameters on the properties of corroded concrete beams using an adaptive neuro-fuzzy inference system (ANFIS)", *Steel Compos. Struct., Int. J.*, **34**(1), 155-170. https://doi.org/10.12989/scs.2020.34.1.155.

Shariati, M., Mafipour, M.S., Mehrabi, P., Ahmadi, M., Wakil, K., Trung, N.T. and Toghroli, A. (2020e), "Prediction of concrete strength in presence of furnace slag and fly ash using Hybrid ANN-GA (artificial neural network-genetic algorithm)", *Smart Struct. Syst., Int. J.*, **25**(2), 183-195. https://doi.org/10.12989/sss.2020.25.2.183.

Shariati, M., Naghipour, M., Yousofizinsaz, G., Toghroli, A. and Tabarestani, N.P. (2020f), "Numerical study on the axial compressive behavior of built-up CFT columns considering different welding lines", *Steel Compos. Struct., Int. J.*, **34**(3), 377-391. https://doi.org/10.12989/scs.2020.34.3.377.

Shariati, M., Tahmasbi, F., Mehrabi, P., Bahadori, A. and Toghroli, A. (2020g), "Monotonic behavior of C and L shaped angle shear connectors within steel-concrete composite beams: An experimental investigation", *Steel Compos. Struct., Int. J.*, **35**(2), 237-247. https://doi.org/10.12989/scs.2020.35.2.237.

Shariati, M., Mafipour, M.S., Mehrabi, P., Shariati, A., Toghroli, A., Trung, N.T. and Salih, M.N. (2020h), "A novel approach to predict shear strength of tilted angle connectors using artificial intelligence techniques", *Eng. Comput.*, **2020**, 1-21. https://doi.org/10.1007/s00366-019-00930-x.

Shen, Z.B., Tang, H.L., Li, D.K. and Tang, G.J. (2012), "Vibration of single-layered graphene sheet-based nanomechanical sensor via nonlocal Kirchhoff plate theory", *Comput. Mater. Sci.*, **61**, 200-205. https://doi.org/10.1016/j.commatsci.2012.04.003.

Shi, J., Chu, L. and, Braun, R. (2019), "A kriging surrogate model for uncertainty analysis of graphene based on a finite element method", *Int. J. Mol. Sci.*, **20**(9), 2355.

https://doi.org/10.3390/ijms20092355.
Sinaei, H., Jumaat, M.Z. and Shariati, M. (2011), "Numerical investigation on exterior reinforced concrete beam-column joint strengthened by composite fiber reinforced polymer (CFRP)", *Int. J. Phys. Sci.*, **6**(28), 6572-6579. https://doi.org/10.5897/IJPS11.1225.
Sinaei, H., Shariati, M., Abna, A.H., Aghaei, M. and Shariati, A. (2012), "Evaluation of reinforced concrete beam behaviour using finite element analysis by ABAQUS", *Sci. Res. Essays*, **7**(21), 2002-2009. https://doi.org/10.5897/SRE11.1393.
Sobhy, M. (2016), "Hygrothermal vibration of orthotropic double-layered graphene sheets embedded in an elastic medium using the two-variable plate theory", *Appl. Math. Model.*, **40**(1), 85-99. https://doi.org/10.1016/j.apm.2015.04.037.
Suhatril, M., Osman, N., Sari, P.A., Shariati, M. and Marto, A. (2019), "Significance of surface eco-protection techniques for cohesive soils slope in Selangor, Malaysia", *Geotech. Geol. Eng.*, **37**(3), 2007-2014. https://doi.org/10.1007/s10706-018-0740-3.
Tahmasbi, F., Maleki, S., Shariati, M., Ramli Sulong, N.H. and Tahir, M.M. (2016), "Shear capacity of C-shaped and L-shaped angle shear connectors", *PLoS One*, **11**(8), e0156989. https://doi.org/10.1371/journal.pone.0156989.
Toghroli, A. (2015), "Applications of the ANFIS and LR models in the prediction of shear connection in composite beams/Ali Toghroli", M.Sc. Dissertation, University of Malaya, Kuala Lumpur, Malaysia.
Toghroli, A., Mohammadhassani, M., Suhatril, M., Shariati, M. and Ibrahim, Z. (2014), "Prediction of shear capacity of channel shear connectors using the ANFIS model", *Steel Compos. Struct., Int. J.*, **17**(5), 623-639. http://dx.doi.org/10.12989/scs.2014.17.5.623.
Toghroli, A., Suhatril, M., Ibrahim, Z., Safa, M., Shariati, M. and Shamshirband, S. (2016), "Potential of soft computing approach for evaluating the factors affecting the capacity of steel–concrete composite beam", *J. Intell. Manuf.*, **29**(8), 1793-1801. https://doi.org/10.1007/s10845-016-1217-y.
Toghroli, A., Shariati, M., Karim, M.R. and Ibrahim, Z. (2017), "Investigation on composite polymer and silica fume–rubber aggregate pervious concrete", *Proceedings of the Fifth International Conference on Advances in Civil, Structural and Mechanical Engineering*, Zurich, Switzerland, September.
Toghroli, A., Darvishmoghaddam, E., Zandi, Y., Parvan, M., Safa, M., Abdullahi, M.A.M., Heydari, A., Wakil, K., Gebreel, S.A. and Khorami, M. (2018a), "Evaluation of the parameters affecting the Schmidt rebound hammer reading using ANFIS method", *Comput. Concrete., Int. J.*, **21**(5), 525-530. https://doi.org/10.12989/cac.2018.21.5.525.
Toghroli, A., Shariati, M., Sajedi, F., Ibrahim, Z., Koting, S., Mohamad, E.T. and Khorami, M. (2018b), "A review on pavement porous concrete using recycled waste materials", *Smart Struct. Syst., Int. J.*, **22**(4), 433-440. https://doi.org/10.12989/sss.2018.22.4.433.
Trung, N.T., Shahgoli, A.F., Zandi, Y., Shariati, M., Wakil, K., Safa, M. and Khorami, M. (2019a), "Moment-rotation prediction of precast beam-to-column connections using extreme learning machine", *Struct. Eng. Mech., Int. J.*, **70**(5), 639-647. https://doi.org/10.12989/sem.2019.70.5.639.
Trung, N.T., Alemi, N., Haido, J.H., Shariati, M., Baradaran, S. and Yousif, S.T. (2019b), "Reduction of cement consumption by producing smart green concretes with natural zeolites", *Smart Struct. Syst., Int. J.*, **24**(3), 415-425. https://doi.org/10.12989/sss.2019.24.3.415.
Wei, X., Shariati, M., Zandi, Y., Pei, S., Jin, Z., Gharachurlu, S., Abdullahi, M.M., Tahir, M.M. and Khorami, M. (2018), "Distribution of shear force in perforated shear connectors", *Steel Compos. Struct., Int. J.*, **27**(3), 389-399. http://dx.doi.org/10.12989/scs.2018.27.3.389.
Willam, K.J. (1975), "Constitutive model for the triaxial behaviour of concrete", *Proc. Int. Assoc. Bridge Struct. Eng.*, **19**(3), 1-30.
Xie, Q., Sinaei, H., Shariati, M., Khorami, M., Mohamad, E.T. and Bui, D.T. (2019), "An experimental study on the effect of CFRP on behavior of reinforce concrete beam column connections", *Steel Compos. Struct., Int. J.*, **30**(5), 433-441. https://doi.org/10.12989/scs.2019.30.5.433.
Xu, C., Zhang, X., Haido, J.H., Mehrabi, P., Shariati, A., Mohamad, E.T., Nguyen, H. and Wakil, K. (2019), "Using genetic algorithms method for the paramount design of reinforced concrete structures", *Struct. Eng. Mech., Int. J.*, **71**(5), 503-513. https://doi.org/10.12989/sem.2019.71.5.503.
Zandi, Y., Shariati, M., Marto, A., Wei, X., Karaca, Z., Dao, D., Toghroli, A., Hashemi, M.H., Sedghi, Y. and Wakil, K. (2018), "Computational investigation of the comparative analysis of cylindrical barns subjected to earthquake", *Steel Compos. Struct., Int. J.*, **28**(4), 439-447. https://doi.org/10.12989/scs.2018.28.4.439.
Zenkour, A.M. (2016), "Nonlocal transient thermal analysis of a single-layered graphene sheet embedded in viscoelastic medium", *Physica E Low Dimens. Syst. Nanostruct.*, **79**, 87-97. https://doi.org/10.1016/j.physe.2015.12.003.
Zhao, X., Fourie, A. and Qi, C.C. (2019), "An analytical solution for evaluating the safety of an exposed face in a paste backfill stope incorporating the arching phenomenon", *Int. J. Min. Metall. Mater.*, **26**(10), 1206-1216. https://doi.org/10.1007/s12613-019-1885-7.
Zhao, X., Fourie, A. and Qi, C.C. (2020a), "Mechanics and safety issues in tailing-based backfill: A review", *Int. J. Min. Metall. Mater.*, **27**(9), 1165-1178. https://doi.org/10.1007/s12613-020-2004-5.
Zhao, X., Fourie, A., Veenstra, R. and Qi, C.C. (2020b), "Safety of barricades in cemented paste-backfilled stopes", *Int. J. Min. Metall. Mater.*, **27**(8), 1054-1064. https://doi.org/10.1007/s12613-020-2006-3.
Ziaei-Nia, A., Shariati, M. and Salehabadi, E. (2018), "Dynamic mix design optimization of high-performance concrete", *Steel Compos. Struct., Int. J.*, **29**(1), 67-75. http://dx.doi.org/10.12989/scs.2018.29.1.067.

CC